The effect of feed water TDS on RO membrane rejection rates and performance

PT du Toit

orcid.org/0000-0003-4941-0820

Dissertation accepted in fulfilment of the requirements for the degree *Master of Engineering in Chemical Engineering* at the North-West University

Supervisor:	Prof HWJP Neomagus
Co-supervisor:	Prof HM Krieg

Graduation:	June 2023
Student number:	12990191

DECLARATION

I, PT du Toit, declare herewith that the dissertation entitled: The effect of feed water TDS on RO Membrane rejection rates and performance, which I herewith submit to the North-West University complies with the requirements set for the degree: Master in Engineering (M.Eng) is my work, has been text-edited in accordance with the requirements and has not already been submitted to any other university.

X

Philip Thomas du Toit
12990191 - 2023-02-28

ACKNOWLEDGEMENTS

I start by thanking and giving the honour to our Father in heaven for the opportunity. Without His grace, strength and divine intervention, this study would not have been possible.

Thank you to my lovely wife. Allowing me to spend weeks away from home taking care of our three toddlers. You are an amazing wife and mother, I am grateful for you in my life.

Prof. Hein Neomagus, you took me under your wing in far from ideal circumstances and for that, I am very grateful. Your excellent guidance made a big impact and your sharp commentary formed the guardrails which kept the work going in the right direction. Thank you for everything.

Prof. Henning Krieg, your support and commitment to this study cannot be ignored and I thank you for that. You provided critical guidance and wisdom at the right times, which helped keep the momentum and belief going when I struggled.

A big think you to my manager, Pieter Myburgh, who supported this work throughout the study and allowed me the time necessary to complete it. The staff at Eskom RT&D for their support and for using their facilities, I would like to specifically mention Tshitso Tamane, Sabelo Senokoane and Kelley Reynolds-Clausen who also fulfilled the role of industrial mentor. Without your, support none of this could have happened

Lastly, I would like to thank the EPPEI (Eskom Power Plant Engineering Institute) programme for acceptance into the program and for providing the opportunity to conduct this study and Eskom for funding this study.

ABSTRACT

Power generation is a major user of fresh water, which is becoming important for Eskom and South Africa due to the water-scarce status. Therefore, the water usage at a thermal power station is a key metric and reverse osmosis (RO) is a key technology that can be used to reduce water consumption. A double pass RO system at a thermal power station used to produce demineralised water for steam production is operating with a large variance in its brackish feed water with total dissolved salts (TDS) ranging between 80 and 1000 mg/L. The reference plant showed a significant decrease in observed salt rejection with lowering feed water concentration. The reason for this decrease in salt rejection was not clear to Eskom and required further investigation.

An experimental test rig was used to study 4” spiral wound membrane modules to replicate the reference plant in a small-scale and controllable setup. The range of feed water concentration was replicated by treating NaCl solutions varying from 10 - 2500 mg/L. Polyamide RO Membranes from three different suppliers (Filmtec™, Toray and Hydranautics) were tested to compare the response in salt rejection to feed water concentration. The test rig was not temperature controlled, and therefore, more than one variable changed during the experimental data collection which requires the development of a model from literature and experimental data to enable the comparison between the membranes on an equal footing. The results produced by the standard salt diffusion equation significantly deviated from the experimental results below 100 mg/L NaCl feed concentrations. This deviation was attributed to the Donnan effect which showed a reduced effect at lower concentrations and subsequently lowers the salt rejection capability of the RO membrane in this region. Therefore, additional terms presented by Anisimov & Orlov (2018) were incorporated into the salt flux equation which then produced a model that predicts the membrane performance throughout the entire feed concentration range that was tested.

The experimental input data is also replicated using the modelling software available from the three membrane suppliers. The results from the software correlated well with the experimental and developed model results. The recommended modifications from an optimisation exercise on the reference plant could allow the plant to be more flexible by achieving maximum recovery over the entire range of feed water qualities. The modifications proposed can potentially allow the reference plant, when operating on the lowest feed water concentration, to increase overall water recovery from 77% to 96%, reduce wastewater by 80% and increase the plant production by 23%.

Keywords: Reverse Osmosis; low TDS; Donnan effect; rejection; permeability; brackish water; modelling; plant optimisation; ultra-pure water

FOREWORD

I have been in the employment of Eskom since 2009 after completing my undergraduate studies in Chemical Engineering. During my first 9 years at Eskom, I was part of the design, construction, commissioning, and operation of this particulate water treatment plant which is the reference plant for this study. Therefore, a lot of the references to the operational information on the reference plant and its purpose within the power station were from my personal experience gained while working in this plant to serve the power station's water requirements.

The inferred why question from the title of this study has been with me since I observed the first operational results of the reference plant in 2015. The explanation for the observed lower salt rejection could not be explained adequately by my initial research, my fellow Eskom colleagues, the plant designers, and the membrane suppliers' representatives. This formed the primary part of the study to find the 'root cause' for the observations made on the reference plant.

The study intends to not only address the theoretical reasons for the lower rejection but to answer the logical follow-up question: How can this be applied to improve the reference plant? Therefore, the study also aims to provide practical answers to the reference plant. The lower salt rejection has a wider impact since the reference plant will be operating with varying feed water quality over a large feed concentration range. From three years of operation experience, it was observed that the plant showed higher rejection values at moderate to higher feed concentrations. Could it be possible that the plant can be optimised to replicate the higher feed concentrations performance with lower feed concentrations? If not, how can it be optimised to adjust to the varying feed concentrations with the reduced salt rejection at lower feed concentrations?

TABLE OF CONTENTS

LIST OF TABLES

LIST OF FIGURES

LIST OF SYMBOLS

B_s	Solute permeability coefficient - L/m^{2}h
b_r	Constant for pressure drop calculation - dimensionless
C	Concentration - mol/L
CP	Concentration Polarisation - dimensionless
d_H	Hydraulic diameter - m
D_s	Solute diffusion coefficient in water – m^2/s
f_{os}	Osmotic conversion factor from mol/L to bar – Lbar/mol
H	Feed spacer thickness - m
J_s	Solute flux - mol/m^{2}h
J_w	Water volumetric flux - L/m^{2}h or LMH
K	Constant for additional solute flux term - mol/m^{2}h
k	Mass transfer coefficient – m/s
L	Length of membrane - m
L_p	Water transport coefficient - L/m^{2}hbar
m_r	Constant for pressure drop calculation - dimensionless
n_c	Number of channels – dimensionless
Q	Volumetric flow rate – L/h
R	Ideal gas constant - Lbar/Kmol
R_o	Observed rejection - %
R_r	Real rejection - %
Re	Reynolds number – dimensionless
Sc	Schmidt number – dimensionless
Sh	Sherwood number – dimensionless
T	Temperature - ºC
Y	Recovery - dimensionless
α	Alpha – constant for Deissler equation
α_B	Alpha – constant for solute permeability coefficient – 1/ºC
α_{Lp}	Alpha – constant for solvent permeability coefficient – 1/ºC
β	Beta – constant for Deissler equation
Δp	Pressure difference - bar
$\Delta\pi$	Osmotic pressure difference - bar
γ	Gamma – constant for Deissler equation
u	Velocity – m/s
ϵ	Void fraction - dimensionless
v	Viscosity – kg/ms
ρ	Density – kg/m^3
Subscripts	
p	Permeate
f	Feed
m	Membrane wall
25	At 25 ºC

CHAPTER 1 INTRODUCTION

Eskom (2021b) owns and operates 91% of South Africa's installed electricity generating capacity and is therefore the biggest role player in its electricity market. In turn, Eskom produces 83.4% of its electricity from coal-fired power stations located in the Mpumalanga and Limpopo provinces the remaining power is produced from 5.8% pumped storage, 5.2% Open cycle gas turbines, 4% Nuclear, 1.2% Hydro and 0.02% from Wind. Coal-fired power stations utilise a significant amount of fresh water, used mainly for cooling purposes and make-up to the boiler and turbine steam cycle. In a water-scarce country such as South Africa, the water usage of a power station becomes an important measure of its performance (Eskom, 2021b) Lower water usage is an indicator of higher efficiency of the power station, a reduction in operating cost and the optimal usage of a scares resource (Eskom, 2018).

Eskom estimated in its 2021 sustainability report that it consumes 2% of South Africa's total freshwater usage, mainly used by its coal-fired power stations. Due to this large impact on the freshwater supply, Eskom has set itself an internal water usage target of 1.3 L/kWh sent out to reduce this in the future (Eskom, 2021a). Targets are aimed to reduce to less than 0.25 L/kWh for the new build stations which is one of the main reasons Eskom installed direct dry cooling condensers on the power units, direct dry cooling utilises fans forcing air through the finned tubes of the condenser. The dry cooling system replaces the use of wet cooling tower and thereby reduces the station water requirement significantly. The water treatment and water balance for the new power stations also form a critical part of the effort to reduce water consumption and their designs incorporated numerous efforts in reducing the station's total water consumption. (Eskom, 2018)

The technology utilised in water treatment is a key factor in its ability to reduce water consumption. The Electric Power Research Institute (EPRI) describes membrane water treatment, specifically RO as a common membrane technology used to reduce water usage and waste production in power plants across the world. EPRI is also of the opinion that RO technology will still be the chief technology in the foreseeable future for water and wastewater minimisation for the power generation industry which means that the optimisation of RO membranes is a critical research topic currently and in the foreseeable future. (EPRI, 2019)

1.1 Background

Water supply to one of Eskom's new power stations located in one of the driest parts of the country is constrained with the currently available source (Water A), which would not be able to meet all the requirements over the power station's lifetime. Therefore, an additional water source (Water B) is required to ensure that the station's water demand is met without compromising the area's human and agricultural water requirements (DOWA, 2008). As a result of using two different water sources, the power station, and its water treatment plant (Plant A) was designed to operate on both water sources A and B. This presented a challenge in the design since the two sources differ significantly in terms of water quality as shown in Table 1-1. (Eskom, 2018)

Table 1-1: Water A and B design values

Constituent	Unit	Water A	Water B
pH	@ 25^0C	8.8	9.1
Electrical Conductivity (EC)	µS/cm @ 25^0C	106.3	950.4
Na^+	mg/L	7.4	100.8
K^+	mg/L	1.6	15.6
M-alkalinity	mg/L as $CaCO_3$	37.6	177.72
P-alkalinity	mg/L as $CaCO_3$	6.9	72.72
Cl^-	mg/L	12	107.6
SO_4^{2-}	mg/L	2.2	89.8
NO_3^-	mg/L	0	4.68
F^-	mg/L	0.2	0.64
Ca Hardness	mg/L as $CaCO_3$	29.1	128.4
Mg Hardness	mg/L as $CaCO_3$	21	119
Total Hardness	mg/L as $CaCO_3$	38.5	247.4
Ba^{2+}	mg/L	0.024	0.1
SiO_2	mg/L	19	4.08
TOC	mg/L	-	9.4

According to the Electric Power Research Institute (EPRI), there are several categories of water qualities commonly encountered in the water treatment industry which are listed in Table 1-2 Water A is a surface water supply and based on the salt concentration it is classified as fresh water with a relatively low Total Dissolved Salts (TDS) (90 (±20) mg/L). Although Water B has a significantly higher TDS (450 (±70) mg/L) than Water A, it is still categorised as freshwater. (EPRI, 2019)

Table 1-2: EPRI water categories encountered in the water treatment industry (EPRI, 2019)

Water category	Total Dissolved Salt (TDS) concentration (mg/L)
Freshwater	< 1000
Brackish water	1000 – 10 000
Highly brackish water (not sea water)	> 10 000
Sea water	25 000 – 40 000

The water treatment plant at the new power station provides process water to all the clean water processes, namely filtered water for auxiliary cooling tower make-up, potable water production for human consumption and fire water alongside its primary function of demineralised water for steam generation. The plant configuration, design capacity and layout are given in Appendix A. The designers of the water treatment plant chose RO as the treatment technology for demineralised water production. This decision was driven by the quality of Water B since the plant should be capable of meeting all its design criteria when operating only on Water B. (Eskom, 2018)

1.2 Plant experience

During the commissioning of the power units, the operators recycled effluent water from the power units to the water treatment plant for demineralised water production which provided an opportunity to evaluate the plant performance over a wide range of feed concentrations. During a 3-year evaluation period leading to this study, the variance of the feed water quality is shown in Figure 1-1. The changes were caused by the ever-changing nature of the process effluent, additional rainwater and mixing between the effluent water and Water A at different ratios at different times.

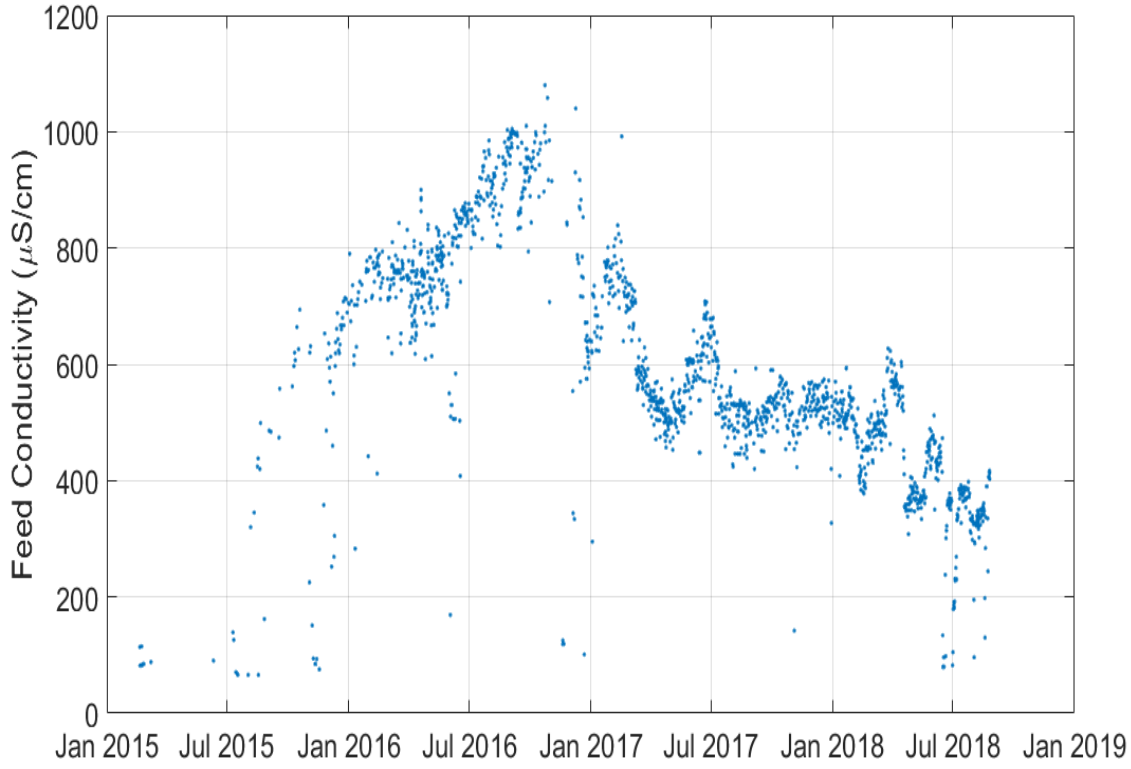

Figure 1-1: Variance of the feed quality while operating on effluent water for 2015 – 2018

Table 1-3 Effluent qualities supplied to Plant A and B compared to Water A and B design values (Eskom, 2018).

Constituent	Unit	Effluent Data 2015 - 2018				Water A Design Value	Water B Design Value
		Average	ST dev	Min	Max		
pH	@25°C	9.1	0.5	8.1	10.3	8.8	9.1
EC	µS/cm @25°C	826.1	61.4	598.0	999.6	106.3	950.4
Na^+	mg/L	17.3	6.4	8.6	35.5	7.4	100.8
K^+	mg/L	103.0	31.2	21.8	188.5	1.6	15.6
M-alkalinity	mg/L as $CaCO_3$	62.6	7.6	37.7	91.9	37.6	177.72
P-alkalinity	mg/L as $CaCO_3$	12.3	7.4	0.0	35.0	6.9	72.72
Cl^-	mg/L	33.7	8.6	15.1	52.5	12	107.6
SO_4^{2-}	mg/L	282.7	27.6	170.1	357.4	2.2	89.8
NO_3^-	mg/L	1.2	1.8	0.0	14.1	0	4.68
F^-	mg/L	1.2	1.2	0.0	4.4	0.2	0.64
Ca Hardness	mg/L as $CaCO_3$	97.4	20.8	67.8	138.0	29.1	128.4
Mg Hardness	mg/L as $CaCO_3$	51.5	18.4	30.1	99.0	21	119
Total Hardness	mg/L as $CaCO_3$	148.3	37.9	99.2	225.0	38.5	247.4
Ba^{2+}	mg/L	0.07	0.08	0.0056	0.818	0.024	0.1
SiO_2	mg/L	14.5	5.1	3.1	38.4	19	4.08
TOC	mg/L	9.5	3.6	5.5	18.3	-	9.4

The effluent water quality supplied to the reference plant is summarised in Table 1-3, from which it was very different in almost all aspects compared to the design specifications for Water A and B. Although the effluent water TDS were similar than Water B the specific ion concentrations differs significantly.

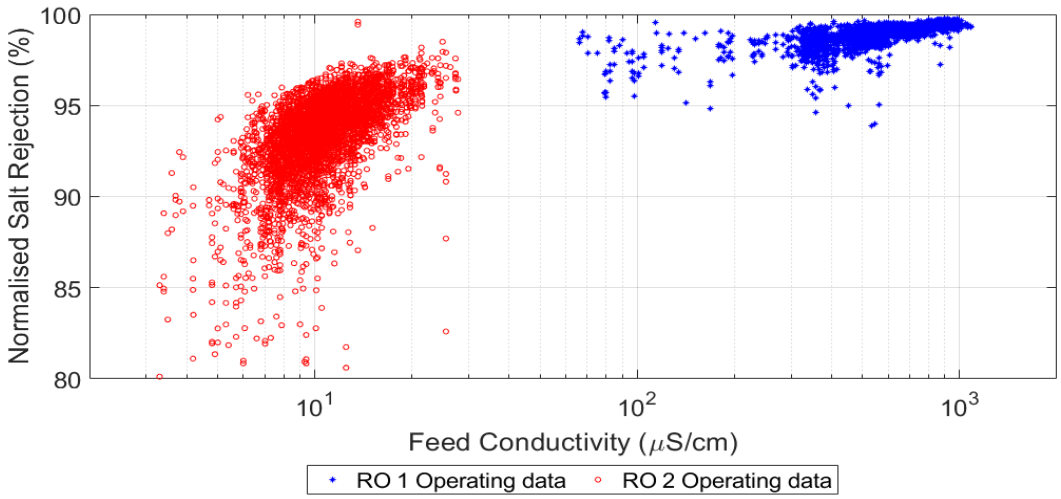

Figure 1-2: Reference plant operating data for RO 1 and RO 2 with design expectations (Eskom supplied data).

The plant performance data from 2015 – 2018 were normalised for temperature and flow variances according to ASTM D4516-19a, and the details of the equations and calculations are given in Appendix B. This normalised salt rejection performance of RO Pass 1 and 2 over the period is shown in Figure 1-2. Most noticeable is the reduction in rejection as the feed water concentration reduces, the rate of decrease changes distinctly at 200 and 30 µS/cm.

The OEM technical documents (DuPont, 2016, 2019, 2022), which were used to design the reference plant, do not detail any physical or chemical aspect of why the rejection of the RO will decrease with decreased feed water concentration. The reference plant design was done at a time when little operational experience was available in Eskom with the operation of a double pass RO system to produce demineralised water. This inexperience meant that the reference water treatment plant was designed with only the worst-case scenario in mind and is not able to adjust for the different feed water qualities. The range of feed concentration demonstrated in Figure 1-2 is significant with RO 1 feed concentration changed with one order and RO 2 another order in magnitude. At the outset of this study, it was also unclear what mechanism or mechanisms are causing the lower rejection with lower feed concentrations. Without this

explanation, the correct plant adjustments or modifications cannot be done to operate the plant at its most efficient point throughout the operating range.

1.3 Problem statement

There is generally not a clear understanding of why there is a reduction in the RO rejection with lower feed concentrations. The reference plant is not able to reach the maximum recovery over the range of expected feed water qualities leading to inefficient operation and wastage of valuable water.

1.4 Aim

This study aims to first determine the membranes rejection capabilities at varying feed concentrations focusing on the lower concentrations using experimentally observed data. Then develop a model to predict the performance throughout the concentration range to assist with understanding the mechanism or mechanisms causing the change in rejection behaviour.

Secondly to evaluate the design of the reference plant, to identify potential modifications that can be made to improve the plant over the wide-ranging feed quality and thereby improve its efficiency.

1.5 Objectives

To support the abovementioned aim, the following objectives are set:

1. Evaluate the rejection and performance of different RO membranes for varying NaCl concentrations with a focus on the low feed concentrations.
2. Develop a model to understand the performance of the current membranes.
3. Benchmark the experimental and model results with membrane suppliers' software results.
4. Review the reference plant and propose modification options to improve the plant's performance for the expected feed water quality range.

1.6 Scope of Study and Limitations

The study focuses on RO membranes operating between 10 and 2000 mg/L feed concentrations. These values were chosen since the reference plant feed for RO 2 has reached as low as 10 mg/L and the RO membranes reference rejection is done with NaCl solution at 1500 or 2500 mg/L.

The test work is done with a single 4” spiral wound membrane and not in the same configuration as the reference plant (all reference to the word membrane refers to the tested 4” spiral wound membrane). Many researchers, with Taniguchi (2001) and Li (2019) as examples, completed their RO studies by only testing a single membrane. Once the performance of the single membrane is known the application thereof can be implemented on any plant configuration using iteration calculations.

The test work will only be done with solutions of NaCl, and not complex water compositions as treated by the reference plant. Taniguchi & Kimura (2000), Jang, *et al*. (2019), Sutzkover, *et al.* (2000), Mickols, *et al.* (2021) and Mai, *et al.* (2019) did experimental work with NaCl as a standardisation salt for determining the mechanisms involved in the performance of RO membranes. It is therefore reasonable to conclude that the observations made with NaCl will also apply to complex waters.

CHAPTER 2 LITTERATURE REVIEW

The literature review starts with a short overview of the global water situation and the role reverse osmosis (RO) membranes play within the current water challenges by giving a brief history of RO membranes followed by an overview of its current place in the market worldwide (Section 2.1). In Section 2.2, the most pertinent physical and chemical aspects related to RO membrane i.e., osmosis, the ion apparent size and the Donnan effect will be discussed. Subsequently, technical details of RO membranes in addition to the necessary modelling equations and considerations are presented in Section 2.3. With this information available, the development of the model, which will be presented in Chapter 3 of this study, can be done. Finally, a conclusion of the most important literature findings is presented in Section 0.

2.1 Background

2.1.1 Water industry

According to the Sustainable Water & Energy Solutions Network report (2021), surface water and groundwater usage have increased by 1% annually since 1980 with surface water representing two-thirds of the total freshwater supply available globally. The other third is supplied by groundwater, which is withdrawn faster than it can be replenished, leading to a reduction in the available groundwater. Most of the global freshwater is used by agriculture (69%) followed by industry including power generation (19%) and lastly households (12%). (SWESN, 2021)

The above-mentioned report predicts that the water sector's energy consumption will increase by 50% in 2030, in part by the ever-growing demand for desalination (the process by which the dissolved mineral salts in water are removed) in both potable water production and industrial usage. The report identified that improving water-use efficiency is key to decreasing water stress worldwide where industries and especially thermal power stations should play an important role. (SWESN, 2021)

2.1.2 History and use of RO membranes

The desalination industry has grown significantly from when the first desalination plants were installed in 1928. Since 2010, the size and number of desalination plants have increased at a steady rate of 6.8% per annum globally with the installed worldwide capacity as of February 2020 standing at 97.2 million m^3/day provided by 20 971 projects. Commercial scale desalination is achieved by mainly two technologies: membrane desalination, which mainly uses RO technology, and thermal desalination attained by either multi-effect distillation (MED) or multi-stage flash (MSF). (Eke *et al.*, 2020)

While the concept of using membranes to use seawater as a source of fresh water was put forth by Hassler in 1949 with the report entitled “The Sea as a source of Fresh Water”, the technology to cost-effectively produce fresh water was not yet available. A breakthrough in the field of membranes was achieved 11 years later when Loeb and Sourirajan developed the cellulose diacetate asymmetric membrane (cellulose acetate – CA). Their membrane exhibited both high flux and a high salt rejection paving the way for commercial and wide-scaled use of membranes. Since then, membrane technology had developed from a mere laboratory tool to a well-developed industrial process where potable and ultrapure water is being produced for industries worldwide. (Shenvi *et al.*, 2015)

The industrialised RO membrane of today is not made from CA anymore but from polyamide (PA) specifically thin film PA. The breakthrough for the PA membrane came in 1985 when Cadotte reported the preparation of a high-performance membrane using in-situ interfacial polycondensation between poly- or monomeric amines and poly- or monomeric functional acid halides. To further improve the performance of the PA membrane, the next stage of development involved crosslinking of these polyamide films, resulting in membranes that had five times higher fluxes and five times better rejection values than the CA membranes.(Shenvi *et al.*, 2015)

Today most PA membranes are of the Thin Film Composite (TFC) type. The current most common chemistry that is used to produce the TFC RO membranes is based on a fully aromatic polyamide (PA) formed by interfacial polymerisation (Wang *et al.*, 2014). Using this method an ultra-thin (100 - 300 nm) PA active layer that controls the separation is produced. To support this thin layer, an intermediate mesoporous polysulfone layer of 30 – 50 µm is added followed by a backing polyester material of 100 – 200 µm (Ding *et al.*, 2014). Since its introduction in the market almost 4 decades ago, the use of TFC membranes has been the major development area to make these membranes more efficient in terms of improved fluxes and salt rejections, while lowering the fouling potential. (Wang *et al.*, 2014)

Eke *et al.* (2020) attributed the success of RO technology in the desalination sector mainly to its significantly lower energy requirement compared to that of thermal desalination. For example, seawater RO (SWRO) and brackish RO (BWRO) use 3-4 kWh/m^3 and 0.5-2.5 kWh/m^3 respectively, compared to the 10-16 kWh/m^3 and 5.5 – 9 kWh/m^3 required by the thermal MED and MSF respectively. However, one of the major drawbacks of RO plants is the membrane fouling potential, where particulates, organic and inorganic compounds, as well as biofouling, are potential foulants that can plague RO plants. To reduce the fouling to cost-effective levels, RO membranes have significant pre-treatment requirements, which increases both the capital and operating costs of RO plants. From the study done by Eke *et al.* (2020), the total cost for SWRO

and BWRO in 2019 ranged between 0.35 to 1.87 $/m^3 and 0.35 to 1.53 $/m^3 respectively. (Eke *et al.*, 2020)

Another important development factor for the rapid increase in efficiency of RO membranes was the development of different membrane modules and configurations such as spiral wound, tubular and hollow fibre that enhanced the separation, provided higher energy efficiencies, and provided configuration flexibility for specific purposes (Shenvi *et al.*, 2015). Of these configurations, the spiral wound membranes are the most widely used in the RO industry, providing a good balance between ease of operation, fouling control, permeation rate and packing density. (Haidari *et al.*, 2018)

Another area of water treatment where RO membranes are replacing older technologies is in the production of ultrapure water. Ultrapure water is artificially cleaned water reducing the contaminants to extremely low levels i.e., typically to the single digit ppb levels. Ultrapure water is typically used in industries such as the semiconductor sector, pharmaceutical manufacturing and the steam cycle make-up water of thermal power plants. (Lee *et al.*, 2016)

Traditionally, ultrapure water applications used ion exchange technology. The early models in the 1970s typically had a configuration consisting of cation exchangers followed by anion exchangers and finally mixed-bed deionisation (MBDI) to reject the residual ionic species. Lee *et al.* (2016) reported that in the previous two decades, both the cation and anion exchangers have largely been replaced by RO membranes. This trend is also evident within Eskom. All the stations that had been built between 1970 and the 1990s have been equipped with Cation-Anion-MBDI plants for demineralised water production. However, all except one of the newer plant installations (since the mid-2000s), had installed RO membranes as the demineralised production technology. (Eskom, 2018)

2.2 Chemical and physical aspects of RO membranes

Having established the relevance of the RO membrane technology for water purification, the chemical and physical aspects influencing the performance of such RO membranes will be discussed to provide a basis for predicting their performance. In this section osmosis, the ion's apparent size and the Donnan effect will be discussed.

2.2.1 Osmosis and reverse osmosis

"*The phenomenon of osmosis is the spontaneous passage of pure solvent into solution separated from it by a semipermeable membrane, a membrane permeable to the solvent but not the solute.*" (Atkins & de Paula, 2002)

If the principle of osmosis is applied to this application, where water is the solvent and dissolved salts are the solutes, and assuming a 100% solute-rejecting membrane, the water will move spontaneously from the low solute concentration side of the membrane to the high solute concentration side of the membrane because of osmosis. The osmotic pressure can then be defined as the pressure that needs to be applied on one side of the membrane to stop the solvent from moving across the membrane spontaneously. (Atkins & de Paula, 2002)

For osmosis to assist in separating dissolved salts from water, a membrane is required which will preferentially allow water to move through while preventing the salts from passing. To overcome the osmotic effect, pressure must be applied to the concentrated side of the membrane which must be greater than the osmotic pressure over the membrane to allow the water to permeate from the high solute concentration to the low solute concentration, hence the origins of the term *reverse* osmosis. When such an applied pressure difference (Δp) is higher than the osmotic pressure difference ($\Delta \pi$) over the membrane, the water molecules will permeate through the membrane producing the desired permeate flow. (Shenvi *et al.*, 2015)

2.2.2 Ion apparent size

The apparent size of an ion in an aqueous solution is significantly larger than the actual size of the ion (ionic radius) itself. This results from the shell of dipolar water molecules forming around the ion, giving the ion a so-called hydrated radius. According to Richard *et al.* (2012), ion transport correlates better with the hydrated radius rather than with the ionic radius (Richards *et al.*, 2012). Tansel describes the hydration shell as $M^{Z+}(H_2O)_n$, where n-number of water molecules are associated in a geometrically defined hydration shell with the ion M having a positive charge of Z (Tansel, 2012).

Tansel (2012) concludes that ions that have a relatively small hydrated radius (e.g. Ca^{2+}, Ni^{2+}) but require relatively high energies to remove the hydration waters, exhibit a sticky behaviour which reduces the ability of such ions to partition into a membrane phase. On the other hand, ions with a relatively small hydrated radius (e.g. K^{+}, Na^{+}), but require relatively low energy to lose the hydration water and can therefore easily partition to the membrane phase, allowing them to permeate across the membrane. (Tansel, 2012)

2.2.3 Donnan effect

The other predominant chemical effect which influences desalination when using RO membranes is the Donnan effect. According to the 2nd law of thermodynamics when contacting two phases or solutions containing completely ionised electrolytes in solution (dissolved salts in water), ion equilibrium must be maintained in each phase or solution. This effect, called the Donnan effect, will prevent any ion from undergoing a phase change or moving through a membrane layer if the solution is not neutral. (Donnan, 1995; Galama *et al.*, 2013; Sengupta & Prakash, 2010)

While the thermodynamic explanation of this effect was first given by Frederic G. Donnan in 1911, the original German paper was translated and published in 1995 under the title of "*Donnan, F. G. Theory of membrane equilibria and membrane potentials in the presence of non-dialysing electrolytes*". Over the years, the Donnan effect has become a well-understood phenomenon which affects not only all living organism cells by regulating ion transport, but also the functioning of nanofiltration (NF) membranes and the performance of RO membranes. (Sengupta & Prakash, 2010)

In RO membranes, the Donnan effect influences the rejection of salts by the membrane, based on the different apparent sizes of both the cations and the anions. If a particulate cation in its hydrated form is too big to pass through the membrane, while a smaller anion could pass through the membrane, the Donnan effect will also prevent the smaller anion from passing through the membrane to maintain the neutrality of the electrolyte solution (balance of charge). (Anisimov & Orlov, 2018).

2.2.4 Membrane surface fouling

Jin *et al.* (2009) defined membrane surface fouling as a decline in separation performance due to accumulation of rejected matter on the membrane surface and surface fouling is generally classified into three mechanisms namely cake, scale, and biofilm formation. Cake formation is caused by convective deposition of organic and colloidal matter on the membrane surface with scale formation results from crystallisation of soluble minerals on the membrane surface and biofilm from the growth of microorganisms throughout the membrane module (Jawor & Hoek, 2009). The Filmtec™ design manual refers to surface fouling caused typically by inadequate pre-treatment, improper materials of construction, failure of chemical dosing systems, inadequate flushing after shutdown, and biological contamination of feed water. The effects of fouling include a decrease in permeate flow and/or a higher solute passage. An increased pressure drop between the feed and concentrate side of the membrane is a common side effect of membrane fouling. (DuPont, 2016)

2.3 Theory and modelling of RO membranes

By understanding and integrating the above-mentioned physical and chemical principles, it is now possible to study the physical operating parameters influencing the operation of RO membranes. Firstly, the factors and properties of the membranes influencing the transport through the membrane in its manufactured form will be discussed in Section 2.3.1. Subsequently, these parameters will be fed into a model to predict the performance of an RO membrane under varying conditions (Sections 2.3.2 - 2.3.3)

2.3.1 Transport parameters

The flux through a membrane can be defined as the membrane's ability to allow the transport of the solvent and solutes through a given area of the membrane. Since the flux is the most significant parameter in terms of the energy requirement of operation, it can be used as a performance measurement to determine and subsequently reduce energy consumption (Okamoto & Lienhard, 2019). The second very important parameter, the rejection or salt passage, can be defined as the membrane's ability to separate solutes of the solution, which is the measurement of the salt removal efficiency of the membrane.

When considering the flux of a system consisting of solutes in a solution, two categories are apparent, the flux of the solution which needs to be high to achieve high energy efficiency (Okamoto & Lienhard, 2019) and the flux of the solutes which should be low to obtain high rejection rates. Note that for this study the solvent is water, and the solute is NaCl.

The water volumetric flux J_w (L/m^{2}h or LMH) is derived from Henry's law and Fick's first law of diffusion and is commonly used in the solution diffusion model and shown in Equation 2-1 (Jang *et al.*, 2019; Wang *et al.*, 2014).

$$J_w = L_p(\Delta p - \Delta \pi) \qquad 2\text{-}1$$

The water transport coefficient L_p (L/m^{2}hbar) denotes the water permeability through the membrane, while Δp (bar) and $\Delta \pi$ (bar) are the pressure, and osmotic pressure differentials, across the membrane. From Equation 2-1, the principle of RO is apparent: water will flow through the membrane (positive flux) if the pressure differential (Δp) is greater than the osmotic pressure difference ($\Delta \pi$) across the membrane, which is referred to as the Net Driving Pressure (NDP) according to Equation 2-2.

$$NDP = \Delta p - \Delta \pi \qquad 2\text{-}2$$

It is clear from Equation 2-1 that the permeability also known as the water transport coefficient (L_p) of the membrane, determines the magnitude of the flux at a given pressure. The permeability is an inherent property of the membrane which is dependent on the design, manufacturing and operating lifetime of its different membrane layers. (Jang *et al.*, 2019)

The osmotic pressure π (bar) can be calculated from the van't Hoff equation given by Equation 2-3

$$\pi = nCR(T + 273.15) \tag{2-3}$$

where C (mol/L) is the concentration, R (Lbar/Kmol) the ideal gas constant, T (ºC) the temperature and n the van't Hoff's factor which is 2 in the case of NaCl. (Atkins & de Paula, 2002)

To calculate the solute flux J_s (mol/m^{2}h), only Fick's law is used in the solution diffusion model, which assumes that the main driving force for the solute flux is the concentration differences across the membrane yielding Equation 2-4. (Wang *et al.*, 2014)

$$J_s = J_w C_p = B_s(C_f - C_p) \tag{2-4}$$

Where C_p (mol/L) is the solute bulk permeate concentration, C_f (mol/L) is the solute concentration of the membrane feed, and B_s (L/m^{2}h) is the solute permeability coefficient (Mai *et al.*, 2019).

The observed rejection (R_o) is calculated from the solute concentration in the feed (C_f) and the solute concentration in the permeate (C_p) according to Equation 2-5.

$$R_o = 1 - \frac{C_p}{C_f} \tag{2-5}$$

The difference between the observed (R_o) and the real (R_r) rejection caused by the concentration polarisation (CP) which is caused by the accumulation of rejected solutes on the surface of the membrane, is one of the most important factors influencing the performance of the of RO membrane separation processes. According to (Jang *et al.*, 2019; Kim & Hoek, 2005; Mai *et al.*, 2019) the thin film theory provides an adequate and practical prediction of the concentration polarisation effect according to Equation 2-6 (Mai *et al.*, 2019).

$$CP = \frac{C_m - C_p}{C_{fb} - C_p} = exp\left(\frac{J_w}{k}\right) \tag{2-6}$$

Where k is the mass transfer coefficient (m/s), C_m (mol/L) is the solute concentration at the membrane surface and C_{fb} (mol/L) the average concentration between the feed and brine (reject).

With this understanding of concentration polarisation and its effect on membrane performance, the real rejection can be defined according to Equation 2-7 (Wang *et al.*, 2014).

$$R_r = 1 - \frac{C_p}{C_m} \tag{2-7}$$

Since CP not only influences the rejection but also the flux, the solute flux equation (Equation 2-4) has to be rewritten to take account of the effect of concentration polarisation as described by the film theory which then yields Equation 2-8.

$$J_s = J_w C_p = B_s(C_m - C_p) \tag{2-8}$$

Finally, the recovery (Y) of the RO membrane can be defined by the ratio (percentage) of the permeate flow (Q_p) to the feed flow (Q_f), given in Equation 2-9.

$$Y = \frac{Q_p}{Q_f} * 100\% \tag{2-9}$$

Since operating parameters such as the feed pressure, temperature and feed concentration influence the performance of the RO operation, any suitable model should be able to accurately predict the influence of such parameters. In Figure 2-1 a graphical display showing the generally expected responses based on brackish and saltwater feed water is presented for the effect of pressure, temperature and feed concentration. (DuPont, 2019)

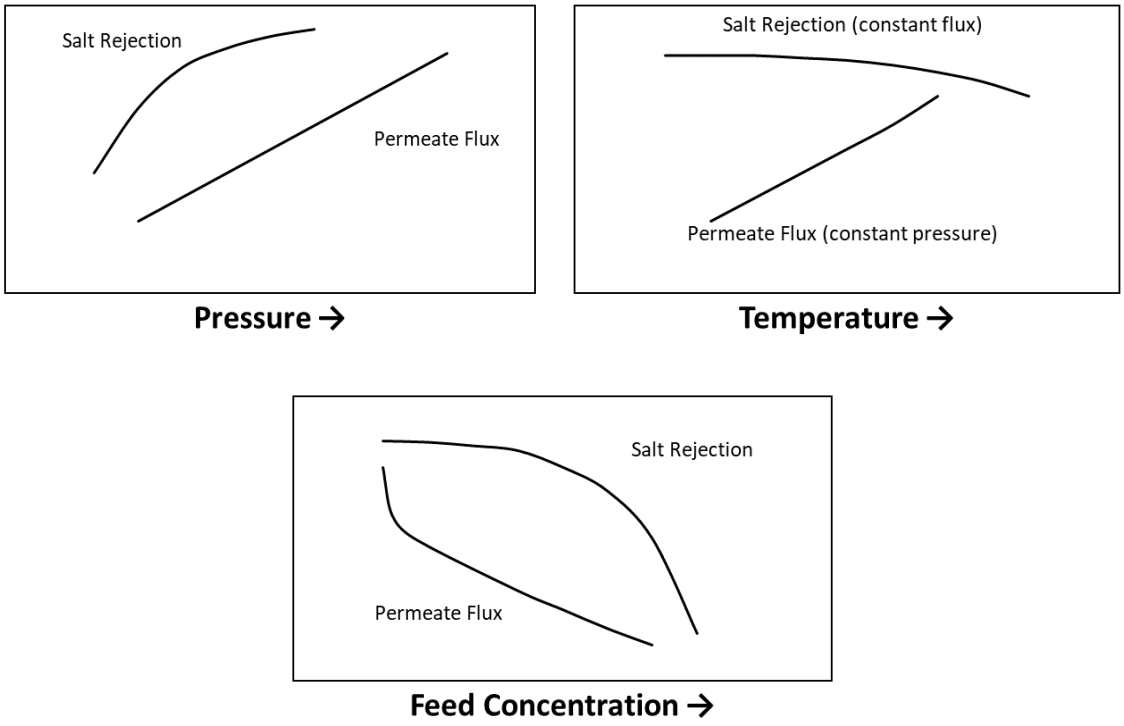

Figure 2-1: Effect of feed pressure, temperature and concentration on an RO membrane performance adapted from DuPont, 2019

According to Figure 2-1, an increase in the feed pressure would normally linearly increase the permeate flux while the salt rejection will initially increase exponentially before reaching a plateau. The linear increase in flux is relatable to Equation 2-1 as the flux is directly proportional to the net driving force or feed pressure. (DuPont, 2019; Hung *et al.*, 2011; Jang *et al.*, 2019; Maddah & Almugahwi, 2017; Mickols *et al.*, 2021)

An increase in temperature will also increase the permeate flux (at constant pressure), while the salt rejection would gradually decrease (at constant flux). With increasing temperature, i.e. increasing energy, the vibration of the molecules in the RO membrane increase, leading to a higher flux of solvent but also a higher flux of solute resulting in the increase in flux and decrease in rejection. (Alsarayreh *et al.*, 2021; Jin *et al.*, 2009; Shen *et al.*, 2016)

With an increase in feed concentration, the permeate flux would decrease, while the salt rejection would remain near constant before reaching a point of exponential decrease (Abdulsalam Ebrahim *et al.*, 2020; Chen & Qin, 2019; DuPont, 2019). At constant pressure, the solvent flux Equation 2-1 supports the fact that the flux will decrease with an increased feed concentration due to the increase in the osmotic pressure. Similarly, the diminishing role of the Donnan effect at increasing concentrations would further reduce the salt rejection at higher feed concentrations. (Anisimov & Orlov, 2018)

Bartels *et al.* (2005) and Ebrahim *et al.* (2020) also observed a decrease in salt rejection with increasing feed concentrations. Both authors showed that the Donnan effect is a critical part of the performance of the RO membrane, where its effect decreases as the concentration increases leading to a reduced rejection when the solute concentration is above 3000 mg/L. Both studies also presented results showing that the Donnan effect is most prominent when the solute concentration in the feed is between 1000 mg/L and 3000 mg/L whereas its effect at concentrations below 300 mg/L is negligible thus leading to a decrease in the salt rejection. (Bartels *et al.*, 2005; Ebrahim *et al.*, 2020)

Based on their results, the expected salt rejection as a function of the feed concentration decreases significantly if the feed concentration is expanded to lower concentrations while gradually decreasing above 2000 mg/L as presented in Figure 2-2. Studies by Hung *et al.* (2011), Ebrahim *et al.* (2020) and Al-Obaidi *et al.* (2018) confirmed that the rejection decreased above 2000 mg/L concur with the decrease in rejection observed by Bartels *et al.* (2005) and Ebrahim *et al.* (2020).

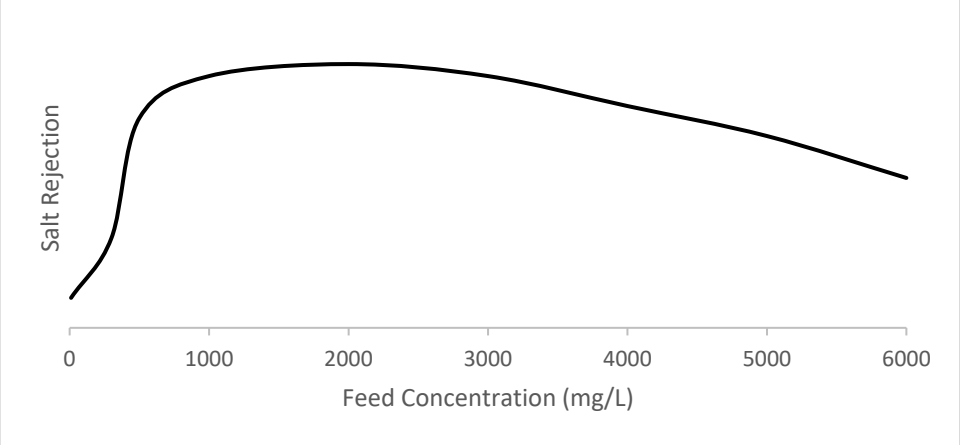

Figure 2-2: Expected salt rejection as a function of the feed concentration for brackish water RO membranes (adapted from Bartels *et al.*, 2005)

2.3.2 Modelling RO Transport Parameters

The two characteristic membrane permeability parameters defined, the water permeability and the solute permeability, are not adequate to fully predict the membrane performance. Equation 2-6, which was used to describe the CP, contains the mass transfer coefficient (k) that has to be calculated. Deissler presented a dimensionless mass transfer correlation for air flow in 1955, according to Equation 2-10 where Sh is the Sherwood number, Re the Reynolds number (see Equation 2-11), Sc the Schmidt number (see Equation 2-14), d_H (m) the hydraulic diameter (see Equation 2-13) and D_s (m^2/s) the solute diffusion coefficient in water (see Equation 2-15).

$$Sh = \alpha Re^{\beta} Sc^{\gamma} = \frac{k d_H}{D_s} \quad 2\text{-}10$$

This correlation was adopted for the modelling of RO membranes by several researchers as shown in Table 2-1.

Table 2-1: Different constants for the dimensionless equation for determining the mass transport coefficient of a membrane

Membrane application	$Sh = \alpha Re^{\beta} Sc^{\gamma}$			**Reference**
	α	**β**	**γ**	
First proposal of the equation	0.023	0.875	0.25	Deissler, 1955
Spiral wound Brackish water membranes. TDS >2500 mg/L	0.020	0.91	0.25	Sutzkover, *et al.*, 2000
Spiral wound membranes with rectangular channels in the feed spacer	0.0096	0.5	0.6	Wang, *et al.*, 2014
Spiral wound seawater membranes	0.080	0.875	0.25	Taniguchi & Kimura, 2000
Spiral wound seawater membranes	0.2	0.57	0.4	Anisimov & Orlov, 2018

For Equation 2-10 (Sherwood number), the Reynolds number (Re) is required, which can be calculated using Equation 2-11.

$$Re = \frac{u d_H \rho}{v} \quad 2\text{-}11$$

Where u is the interstitial velocity (m/s), d_H the hydraulic diameter (m), ρ the density (kg/m^3) and v the dynamic viscosity (kg/m.s). u can be calculated with Equation 2-12 using the inlet volumetric flow rate (Q in L/h) divided by the number of channels (n_c), spacer height (H in m), the void fraction (ϵ) and the length (L in m) of the membrane. (Li *et al.*, 2016)

$$u = \frac{Q}{n_c H \epsilon L} \quad 2\text{-}12$$

Several correlations can be used to determine the hydraulic diameter (d_H) with the most commonly used given in Equation 2-13 (Srivathsan *et al.*, 2014), where the feed spacer thickness is normally stated in the membrane datasheet often presented in the unit "*mil"* which is an empirical unit equal to one-thousandth of an inch.

$$d_H = 2 * Feed\ spacer\ thickness \tag{2-13}$$

The Schmidt Equation 2-14 is used to calculate the Schmidt number (Sc) where v is the dynamic viscosity in kg/m.s and ρ the density in kg/m^3.

$$Sc = \frac{v}{\rho D_s} \tag{2-14}$$

Finally, according to Taniguchi, *et al.* (2001), the diffusion coefficient D_s can be determined using Equation 2-15, with C being the feed concentration in kg/m^3 and T is the temperature in ºC.

$$D_s = 6.725 \cdot 10^{-6} \cdot exp\left(0.1546 \cdot 10^{-3} \cdot C - \frac{2513}{273.15 + T}\right) \tag{2-15}$$

2.3.3 Temperature correction

It was mentioned previously that RO membranes are sensitive to temperature changes with a typical operating range of 5 to 35 ºC. Therefore, the parameters of the membranes have to be corrected for the temperature used (DuPont, 2019). Li (2019) and Taniguchi (2001) presented Equations 2-16 and 2-17 to calculate the water transport coefficient (L_p) and solute permeability coefficient (B_s) as a function of the temperature.

$$L_p = L_{p25} exp\left(\alpha_{Lp}(T - 25)\right) \tag{2-16}$$

$$B_s = B_{s25} exp\left(\alpha_B(T - 25)\right) \tag{2-17}$$

For both equations, L_{p25} and B_{s25} represents the transport and permeability coefficients at 25 ºC. The constants α_{Lp} (1/ºC) and α_B (1/ºC) represent the dependence on temperature change for each parameter and can be obtained from the experimental data.

2.3.4 Modified solvent flux equation

The work presented by Bartels *et al.* (2005), Galama *et al.*(2013) and Anisimov & Orlov (2018) has shown that the behaviour of RO membranes changes significantly at lower feed concentrations. During the model work of the experimental data obtained in this study (see Section 4.3), it became apparent that the solution diffusion model presented in Section 2.3.2 could

not accurately model the experimental results for feed concentrations below 100 mg/L (1.71×10^{-3} mol/L).

Anisimov & Orlov (2018) investigated the salt rejection characteristics of an RO membrane at feed concentrations as low as 5 mg/L of various electrolyte solutions (NaCl, Na_2SO_4, $CaCl_2$, $MgCl_2$ and $FeCl_3$). The experimental results confirmed the results presented by Bartels *et al.* (2005). A correlation between the membrane wall concentration (C_m – mol/L) and the salt permeability coefficient (B_s in L/m^{2}h), represented in Equation 2-18, containing b_1, b_2 and b_3 which are constants at low feed concentrations was found.

$$B_s = \frac{b_1}{C_m} + \frac{(C_m)^{b_2}}{b_3} \qquad 2\text{-}18$$

Anisimov & Orlov (2018) determined that in the region where the membrane wall concentration (C_m) tends towards zero, the salt flux (J_s) is equal to b_1 while the second term becomes insignificant. It was also found that b_1 correlates to the sum of the hydration numbers of the electrolyte ions. Subsequently, two methods to determine the hydration numbers (n_{Wi}) that can be used for the correlation. For this study, only the second method, shown by Equation 2-19, will be used as the input data is easily obtained. (Anisimov & Orlov, 2018)

$$n_{Wi} = \frac{({r_{hi}}^3 - {r_{ci}}^3)}{{r_w}^3} \qquad 2\text{-}19$$

r_{hi} is the hydration shell radius (Å) and r_{ci} the ionic radius (Å) and r_w (1.38 Å) the radius of the water molecule in Å. The radii for Na^+ and Cl^- that were used in this study are given in Table 2-2.

Table 2-2: Table of ionic radii used in this study (Tansel, 2012)

	Radius (Å)	
	Ionic	**Hydrated**
Na^+	0.99	2.76
Cl^-	1.81	3.24

Anisimov & Orlov (2018) presented an expanded equation for determining the salt flux (J_s) with ${J_{si}}^D$ and ${J_{si}}^K$ the diffusive (Equation 2-20) and convective (Equation 2-21) electrolyte fluxes respectively. Both fluxes are dependent on the pressure difference over the membrane and the membrane wall concentration.

$${J_{si}}^D = B_s(C_m - C_p) \qquad 2\text{-}20$$

$${J_{si}}^K = b_1 C_m(\Delta p - \Delta\pi) \qquad 2\text{-}21$$

Anisimov & Orlov (2018) further showed that the relationship between ${J_{si}}^{D}$ and the feed concentration's were offset relative to zero, while there was no offset in the relationship between ${J_{si}}^{K}$ and the feed concentration. Based on this observation, they assigned ${J_{si}}^{F}$ as the contribution of salt flux at lower feed concentrations, which they termed the additional salt flux (Equation 2-20). They demonstrated that this additional flux was not dependent on the convective or the diffusive driving forces. Therefore, they were able to correlate ${J_{si}}^{F}$ to the hydration numbers (n_{Wi}) as shown in Equation 2-22 where K is a dimensionless constant that is determined from the experimental data. (Anisimov & Orlov, 2018)

$$ {J_{si}}^{F} = \frac{K}{\sum n_{Wi}} \qquad 2\text{-}22 $$

The additional salt flux term ${J_{si}}^{F}$ will become insignificant small compared to the other two salt fluxes at higher feed concentrations, i.e. above 200 - 300 mg/L. Based on this, Equation 2-8 for solute flux can now be expanded including the additional terms yielding Equation 2-24 with b_1 and K as additional constants to be determined experimentally.

$$ J_{si} = {J_{si}}^{D} + {J_{si}}^{K} + {J_{si}}^{F} \qquad 2\text{-}23 $$

$$ J_{si} = B_s\left(C_m - C_p\right) + b_1 C_m(\Delta p - \Delta\pi) + \frac{K}{\sum n_{Wi}} \qquad 2\text{-}24 $$

Equation 2-24 represents the modified solute flux equation which is the expansion on the standard solute flux equation (Equation 2-4) in the solution diffusion model. The modified equation allows for the reduction in the Donnan and therefore to accurately predict the membrane performance at lower TDS values.

2.4 Conclusion

In summary, the literature study first showed the importance of RO in the water treatment industry and specifically to this study's application in the field of ultra-pure water production. Secondly, it identified the critical operating parameters that influence the RO performance are feed flow, pressure, temperature, and concentration and that any model will have to be able to account for each of these variances adequately.

The solution diffusion model presented in Sections 2.3.1 to 2.3.3 only adequately describes the influence of flow, pressure, and temperature, not the complete range of feed concentrations. Therefore, additional equations and constants are required and presented in Section 2.3.4 to model the reduction in the Donnan effect with lower feed concentrations.

With the information provided in this chapter, the experimental setup and modelling of the data can be developed.

CHAPTER 3 EXPERIMENTAL AND MODELLING

To evaluate the membrane rejection over a wide feed concentration regime, a controlled environment is required where the main process parameters can be varied. Therefore, an experimental setup was designed to vary the parameters and enable the measurement of the membrane performance to provide data for modelling purposes.

Chapter 3 details the experimental and modelling starting with Section 3.1 which provides the rationale for the scope of the experimental setup. The design of the experiment is given in Section 3.2 along with the measurements done during the test work. Section 3.3 provides the details of the model development to complete the modelling of the data while details of the experimental program are listed in Section 3.4. The chapter is concluded in Section 3.5.

3.1 Experimental concept

Most RO plants install multiple membranes in series, arrays, and stages, as demonstrated by the reference plant in this study (Li, 2012, 2019; Zhangxin Wang, 2020). Changes to the configuration do not change the membrane characteristics, but only the feed conditions to each membrane will be different. Therefore, only a single membrane will be tested. Jang *et al.* (2019); Mai *et al.* (2019); Mickols *et al.* (2021); Sutzkover *et al.* (2000); Taniguchi & Kimura (2000) did experimental work with NaCl as a standardisation salt to determine membrane transport parameters. Coupled with the fact that the RO industry determines the reference rejection with standardised NaCl solution (1500 or 2000 mg/L) it was decided that test work for this study will only be done with NaCl solutions at different concentrations.

Seven different NaCl concentrations were made-up to provide data over the applicable concentration range. The test work was repeated with 3 membrane suppliers' brackish water RO membranes. Membranes from DuPont (Filmtec™ BW30-4040), Toray (TM700D) and Hydranautics (CPA7-LD-4040) were used. The relevant properties of each membrane are listed in Table 3-1.

Table 3-1: Membrane properties from supplier information

Membrane properties	Filmtec^{TM} BW30-4040	Toray TM710D	Hydranautics CPA7-LD-4040
Membrane Polymer	Polyamide Thin-Film composite	Cross Linked Fully Aromatic Polyamide Composite	Composite Polyamide
Minimum Salt Rejection in reference to NaCl	99.50%	99.65%	99.80%
Supplier Rejection Test conditions	2000 ppm NaCl, 10.3 bar applied pressure, 25 ^{o}C, 15% recovery	2000 ppm NaCl, 15.5 bar applied pressure, 25 ^{o}C, 15% recovery	1500 ppm NaCl, 15.5 bar applied pressure, 25 ^{o}C, 15% recovery
Membrane Active area	7.2 m^2	8 m^2	7.43 m^2
Feed spacer thickness	34 mil	31 mil	34 mil
Permeate flow rate	9.5 m^3/day	9.8 m^3/day	8.71 m^3/day
Membrane length	962.6 mm	962.6 mm	962.6 mm
Maximum recovery	15%	15%	15%
Number of channels (n_c)	23	23	23
Void fraction (ϵ)	0.905	0.905	0.905
Length (L)	0.94 m	0.94 m	0.94 m

3.2 Experimental layout

The Eskom research facility has an already constructed test skid consisting of several water treatment technologies, including an RO section, which was made available to complete the experimental work. Figure 3-1 shows a Process and Instrumentation Drawing (P&ID) of the relevant section of the test skid (Eskom, 2018). The rig was set up during the test in such a way that a solution of a certain concentration or mixture can be made up and then passed through the membrane with the permeate and reject recycled to the feed tank. This allowed the skid to reach a steady state condition to determine the performance of the membranes.

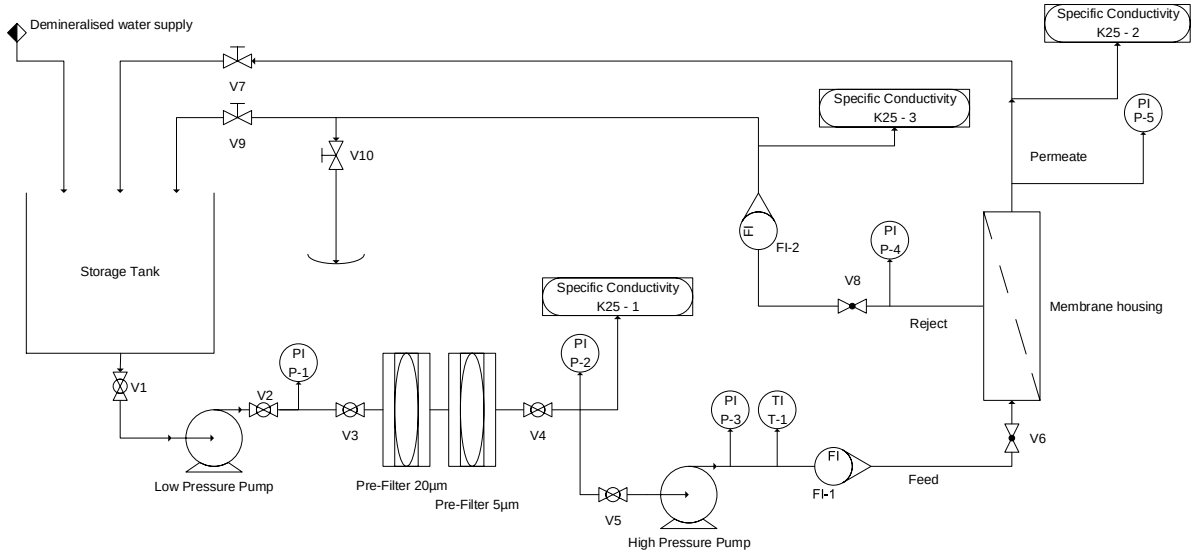

Figure 3-1: Process and Instrumentation Drawing for the experimental setup (Adapted from Eskom (2018).

The storage tank (180 L) was used as a buffer tank filled from the research facility's demineralised production plant to flush newly installed membranes and prepare the solutions to the desired concentration. The feed water to the membrane was filtered using 20 and 5 µm pleated cartridge filters to ensure the feed water SDI (Silt Density Index) of < 5 requirements were met during the testing. The filtered feed water was supplied to a single 4" spiral wound membrane inside an FRP (fibre-reinforced plastic) membrane pressure vessel. The test skid was equipped with a low-pressure pump (Grundfos CM5, 4.7 m^3/h at 37 m [3.7 barg]) before the pre-filter, and the high-pressure pump (Grundfos CRN, 1 m^3/h at 110 m [11 barg]) for the RO membranes feed. The feed water flow rate was controlled with a manual valve (V6) after the high-pressure pump and the recovery over the skid was controlled with a manual valve (V8) at the reject outlet. All piping, valves and fittings were PN-16 PVC (polyvinyl chloride) material.

Rotameters (FI-1 [Georg Fischer short version 200 – 2000 L/h] and FI-2 [Georg Fischer short version 100 – 1000 L/h]) are installed on the feed water and reject lines. The rotameters did not measure the flow accurately enough therefore, the permeate and reject flow were measured using a bucket, stopwatch and scale (Adam WFK150) to determine the flow used for flux and recovery calculations. The stream was diverted into the bucket for a minimum of 25 seconds to get an average flow measurement. The time and weight of the water were then used to determine the flow rate and the collected water was returned to the feed tank. The various concentrations, is continuously monitored by the conductivity meter, so that potential water losses (by evaporation) (open tank cover) will not impact the experimental results.

Pressure gauges (P-1 and P-2) are installed before and after the pre-filter to monitor the condition of the filters. Two WIKA CPG1500 digital gauges (0 to 16 barg and -1 to 1.5 barg) were used to measure the feed, reject and permeate pressures at PI-3, PI-4 and PI-5 by moving the high-pressure gauge between the feed and reject points. The high-pressure gauge was moved between the feed and reject streams for the data points when both points were measured, only one high-pressure CPG1500 was available.

The feed water before pre-filtration (K25-1) and permeate stream (K25-2) was continuously sampled via online analysers measuring the specific conductivity. The feed stream used a Swan AMI Silicon4 with the Swansensor Shurecon P conductivity probe accurate to 0.5% of the reading for the conductivity. The analysers are equipped with the Swan nonlinear function for natural waters temperature compensation for conductivity using a PT1000 temperature sensor. The permeate stream used a Swan AMI Inspector Conductivity with a UP-Con1000SL and integrated PT1000 temperature probe used for conductivity measurement (also with temperature compensation of the conductivity based on the Swan nonlinear function for high-purity waters (Wagner, 2012)). All collected sample flows were returned to the storage tank to keep the volume and concentrations unchanged during the measurement.

The RO feed water temperature was taken as the temperature measurement of the feedwater measured by the Swan AMI Silicon4. The experimental setup is open to the environment with only a roof structure. The setup is also not equipped with any form of temperature control therefore, the temperatures varied during the collection of the experimental data.

The experimental rig was limited in terms of flow capacity therefore, the membranes could only be operated up to 45% of their allowed operating flux. The membrane with the lowest flux at the maximum allowable recovery (15%) could treat up to 2419 L/h feed water flow. The Eskom facility was designed to treat 1000 L/h feed water and all the pumps were sized according to this requirement and therefore, the maximum feed flow that could be achieved was 1200 to 1300 L/h.

3.2.1 Experimental operating conditions

Each new membrane was flushed with demineralised water for at least 2 hours before the permeate and reject were recovered to the feed tank as per the supplier's recommendations. The membranes that were stored in <1% SMBS (Sodium metabisulphite) preservation fluid were flushed until the permeate flow conductivity was at least less than the demineralised feed concentration. Each membrane was first operated at various temperatures (as the water temperature changed with the ambient) with pure water (<2 µS/cm) to collect data for the determination of the permeability coefficient and its temperature dependence curve.

NaCl (CAS – 7647-14-5) was purchased from Associated Chemical Enterprise (ACE) with a minimum purity of 99.5%. The NaCl solutions were made-up between 10 to 2300 mg/L, starting at the lowest concentration. At each concentration point, 3 measurements were taken at the highest flux and then 3 measurements at a lower flux. A minimum of 3 measurements were taken for each of the solutions prepared and were repeated for all 3 membranes.

After the experimental runs were completed the NaCl solutions were washed into the storm water drain facilities since the water quality, diluted with the flushing demineralised water had a TDS similar to that of potable water. The used membranes were disposed of via the Eskom hazardous waste removal contract.

3.2.2 Data measurements

Data collected during each experimental run where: Permeate flow rate (L/h), Reject flow rate (L/h), Feed conductivity (µS/cm), Permeate conductivity (µS/cm), Feed water temperature (°C), Feed pressure (kPa), Reject pressure (kPa) and Permeate pressure (kPa). For the NaCl solutions, only the online analysers were utilised for data collection and the conductivity values were converted to TDS using a factor calculated from the molar conductivities. Using the molar conductivities for Na^+ and Cl^- as 0.05011 and 0.07635 SL/molcm respectively, the factor calculated to convert from mg/L NaCl to µS/cm is 2.164. (Atkins & de Paula, 2002)

A sample calculation and experimental measurement repeatability of the raw data are shown in Appendix C.1 and C.2 respectively. A repeatability value for the 95% probability is calculated according to a method given by Mandel and Lashof (1987) for one set of the Hydranautics data. The repeatability value (r) for the feed flow is 3.2 L/h, reject flow is 11.2 L/h, the feed conductivity is 6.4 µS/cm and the permeate conductivity 0.1 µS/cm. The permeate conductivity is very low due to the very small variance in between measurements (s = 0.03).

The average standard deviation calculated from the sample calculation for the feed conductivity is 2.3 µS/cm and the permeate conductivity 0.03 µS/cm. Using the propagation of the error calculations with the rejection equation (Equation 2-7) the standard deviation of the rejection calculation is 0.01%. The average standard deviation for the permeate flow was calculated to be 1.2 L/h. The permeate flow and rejection is the two reported parameters and both standard deviations are smaller than the data point on the figures therefore the error bars would not be visible. Furthermore, the model calculation already accounted for the deviations by calculating the parameters with all available data points. Based on this information it was decided that the standard deviations will not be shown in the reported results.

3.3 Data Modelling

3.3.1 Modelling philosophy

To develop a model for predicting the RO performance the pressure difference over the reject channel is first modelled to determine the average pressure difference ($\Delta\bar{P}$) and operating pressures. Secondly, the water and solute flux are determined which requires the water transport coefficient (L_p) and the solute permeability coefficient (B_s) with temperature correction. Thirdly the mass transfer coefficient (k) is calculated from the Deissler equation (Equation 2-10) and therefore the values for α, β and γ need to be known for the applicable membrane. The experimental data were then used to determine the required constants as input into the model. (Li, 2019)

The philosophy of the modelling calculation described in the following sections was mostly developed from the work done by Mingheng Li in 2019 who studied and modelled seawater spiral wound membranes from experimental data done by Avlonitis *et al.* (1991). Li (2019) developed the reject pressure difference equation from the first principles with the assumptions proved in previous work presented by Li (2012) and Li (2016). The calculation for determining the membrane wall concentration was also determined by Li (2019).

The basis of the mass transfer modelling calculation is also from Li (2019). The additional equations for the average salt flux ($\bar{J}_s$) developed by Anisimov & Orlov (2018) and a fouling factor to the average water flux ($\bar{J}_w$) were added (DuPont, 2016). Calculating these parameters using a single experimental data point provides non-sensible values. The same results were found by various other researchers (Chen & Qin, 2019; Hyung & Kim, 2006; Li, 2019; Taniguchi *et al.*, 2001). All these studies showed that experimental and operational data of several operating points must be used with an optimisation calculation to determine the membrane parameters.

3.3.2 Modelling Reject Pressure difference

In Equation 3-1 Li (2019) developed an equation for modelling the reject pressure difference over a spiral wound membrane. Dimensionless constant b_r assumes that the velocity impact is directly related to the feed flow rate of the membrane therefore, b_r represents the friction factors related to the pressure drop with m_r another constant to be determined from experimental results (Li, 2019).

$$P_F - P_R = \frac{b_r}{3 - m_r} v^{m_r} \frac{{Q_R}^{3-m_r} - {Q_F}^{3-m_r}}{Q_R - Q_F} \qquad 3\text{-}1$$

P_F and P_R are the feed and reject pressures (bar), Q_R and Q_F the feed and reject flow rate (L/h) and ν is the kinematic viscosity (m^2/s) of water at feed pressure and temperature. Using data points where the feed and reject pressure and flow rates were available the dimensionless constants b_r and m_r were determined for each membrane using optimisation calculation (MATLAB® function fminsearch).

Li (2019) developed Equation 3-2 to calculate the average reject pressure difference ($\bar{P}_r$). The recovery (Y) is calculated from the permeate and feed flow rate, as given in Equation 3-3 and m_r is determined in Equation 3-1.

$$\bar{P}_r = P_F + (P_R - P_F)\frac{1 + \frac{(1-Y)^{4-m_r} - 1}{\frac{4-m_r}{Y}}}{1-(1-Y)^{3-m_r}} \quad 3\text{-}2$$

$$Y = \frac{Q_P}{Q_F} \quad 3\text{-}3$$

Due to the relatively low permeate flow, the permeate pressure drop for this study was assumed to be negligible, this assumption is confirmed by Li (2012).

3.3.3 Modelling Water Permeability

The experimental data with pure water (demineralised water) at varying temperatures and flux were used to determine the membrane water transport coefficient L_p. When pure water is supplied to the membrane the osmotic pressure can be set to zero; therefore Equation 2-1 can be simplified to Equation 3-4 which is used in determining the water transport coefficient.

$$L_p = \frac{J_w}{\Delta\bar{P}} \quad 3\text{-}4$$

The coefficient is temperature dependent, demonstrated by Taniguchi & Kimura (2001) and Li (2019). For each membrane, the temperature-dependent curve of the water transport coefficient was determined according to Equation 3-5, with the water transport coefficient at 25 ºC being L_{p25} (L/m².h.bar), T is temperature in °C and α_{Lp} in 1/ºC.

$$L_p = L_{p25} exp\left(\alpha_{Lp}(T-25)\right) \quad 3\text{-}5$$

3.3.4 Modelling the Mass Transfer Coefficient

To determine the mass transfer coefficient (k) the solute concentration at the membrane wall (C_m) must first be determined. Li (2019) also developed an equation for calculating the average membrane wall concentration ($\bar{c}_m$) which is given by Equation 3-6.

$$\bar{c}_m = -c_F \frac{\ln 1 - Y}{Y} - \frac{b_m J_w c_f (T + 273.15)^{\gamma-1} \nu^{\beta+1-2\gamma}}{\beta Y {Q_F}^{\beta}} \left(1 - \frac{1}{(1-Y)^{\beta}}\right) \quad 3\text{-}6$$

Constants b_m, β and γ can be experimentally determined, with β and γ also the constants from the Deissler mass transfer Equation (Equation 2-10).

The average salt flux ($\bar{J}_s$), average solute flux ($\bar{J}_w$) and the salt permeate coefficient (B_s) are determined simultaneously using Equations 3-7, 3-8, 3-9 and 3-10. The average salt flux used in Equation 3-7 is the modified solution diffusion equation discussed in Section 2.3.4.

$$\bar{J}_s = B_s(\bar{c}_m - \bar{c}_p) + b_1 \bar{c}_m \left[(\bar{P}_r - P_p) - f_{os}(\bar{c}_m - \bar{c}_p)\right] + {K}/{n_{Wi}} \quad 3\text{-}7$$

$$\bar{J}_w = L_p \left[(\bar{P}_r - P_p) - f_{os}(\bar{c}_m - \bar{c}_p)\right] * FF \quad 3\text{-}8$$

$$B_s = B_{s25} exp\left(\alpha_B (T - 25)\right) \quad 3\text{-}9$$

$$f_{os} = nR(T + 273.15) \quad 3\text{-}10$$

With f_{os} a conversion factor for concentration (mol/L) to osmotic pressure (bar), n is 2 for sodium chloride, R is 0.0834147 (Lbar/Kmol) and FF is a dimensionless fouling factor between 0 and 1. For membranes operating at the nominal flow rate (no fouling), the factor will be 1, as the membrane water permeability decreases due to fouling the factor is adjusted to less than 1. (DuPont, 2016)

Using the experimental data an optimisation calculation is done with Equation 3-6 to 3-10 in MATLAB® to determine the constants B_{s25}, α_B, b_m, β, γ, b_1 and K with Equation 3-11 set as the objective function.

$$Min = \sum_i \left(1 - \left(\frac{J_w^{mod}(i)}{J_w^{eks}(i)}\right)^2\right) + \sum_i \left(1 - \left(\frac{J_s^{mod}(i)}{J_s^{eks}(i)}\right)^2\right) \quad 3\text{-}11$$

The superscript *mod* refers to the flux values calculated from the model and *eks* the values calculated from experimental work.

The only outstanding constant for the model is α of the Deissler equation (Equation 2-10), to determine α a separate calculation is required. Firstly, the mass transfer coefficient (k) is calculated from the experimental data ($kdata$) by using the now-known average wall concentration ($\bar{c}_w$) as input into the concentration polarisation (CP) equation (Equation 2-6). By guessing a value for α as input into the Deissler equation a model mass transfer coefficient ($kmodel$) is calculated. Using the two mass transfer coefficients as input into an optimisation calculation using Equation 3-12 as the goal the final value of α is determined.

$$f_{min} = \sum_i (kdata_i - kmodel_i)^2 \qquad 3\text{-}12$$

3.3.5 Calculating results from model data

Once the modelling parameters and characteristics are known for a specific membrane the membrane performance for a set of given operating conditions can be predicted. Given the operational temperature (T), feed pressure (P_f), feed flow rate (Q_f), feed salt concentration (C_f) and permeate pressure (P_p) the following procedure was used to predict the performance of the membrane.

1. Assume a permeate flow rate Q_{pguess} and permeate concentration C_{pguess}
2. Determine the water permeability (L_p - Equation 3-5) and salt permeability (B_s – Equation 3-9) for the given temperature.
3. Calculate recovery $Y = Q_{pguess}/Q_f$ and brine flow rate $Q_r = Q_f - Q_{pguess}$
4. Calculate the reject outlet pressure and the average pressure difference from Equations 3-1 and 3-2.
5. Calculate the water flux $J_w = Q_{pguess}/A_{membrane}$
6. Calculate the mass transfer coefficient (k) using the Deissler Equation 2-10
7. Manipulate Equation 2-6 and calculate the wall concentration C_m using C_{pguess}.
8. Calculate the water flux J_{wm} using Equation 2-1 using the calculated C_m and C_{pguess}.
9. Calculate the salt flux J_s using Equation 2-24
10. Calculate the permeate concentration with $C_p = J_s/J_{wm}$
11. Iterate Q_{pguess} and C_{pguess}.until $(1 - \left(\frac{J_w}{J_{wm}}\right)^2) < 10^{-6}$ and $(1 - \left(\frac{C_p}{C_{pguess}}\right)^2) < 10^{-6}$

The above steps are also visually represented below in Figure 3-2. To handle a large amount of data the calculation was done using the MATLAB® nonlinear solver function $solve$.

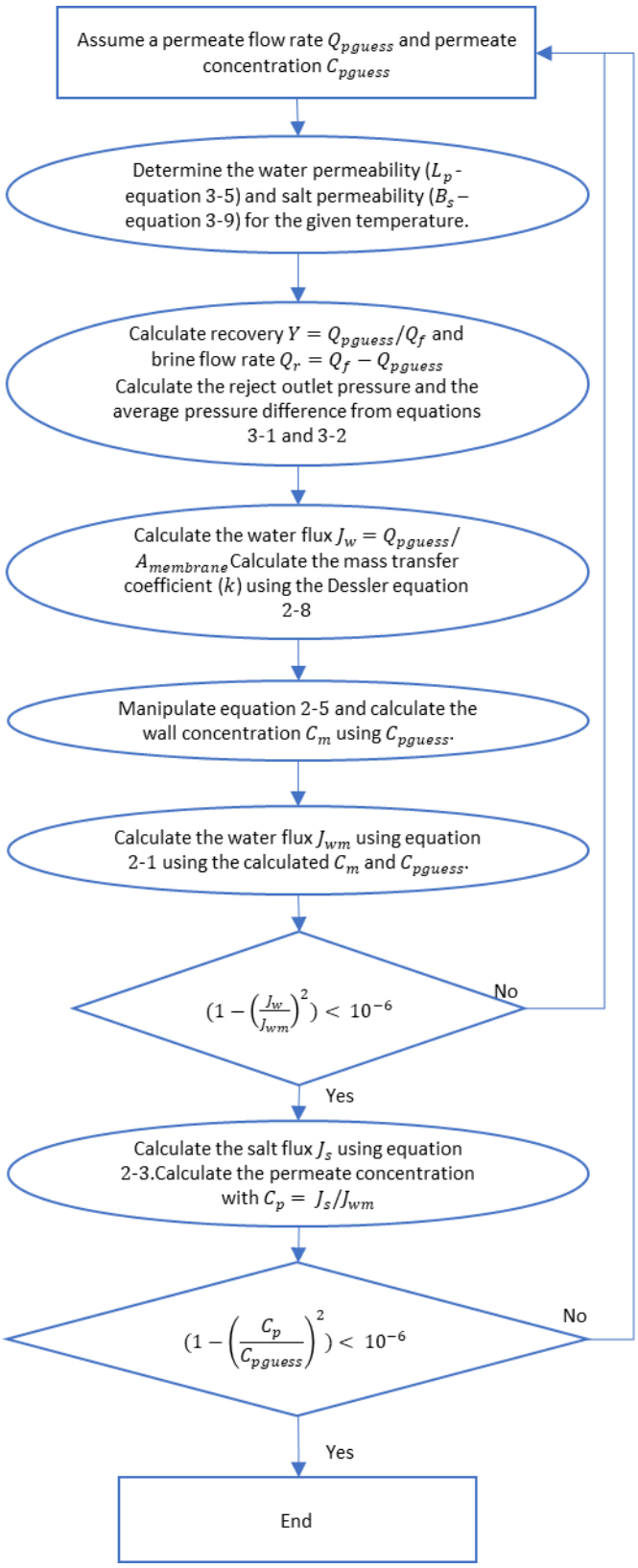

Figure 3-2: Visual diagram for the calculation procedure

3.4 Experimental program

The experimental setup was utilised to produce data for 3 different membranes, the used data points and dates for the results are summarised in Table 3-2. Only two Filmtec™ membranes were available for testing. The first membrane was used to test and optimise the experimental setup. When the second membrane was installed the rejection results observed were very low and after fault finding was done it was determined that the membrane must be defective, and the results could not be used. Therefore, only the data points listed in Table 3-2 were sampled with the correct experimental method and could be used. Both the Filmtec™ and Hydranautics membranes were dry stored in between data sets to simulate fouling conditions which are typically expected to occur in the long-term operation of industrial applications. This data is used to determine if the model can be used with the fouling factor (FF). In the case of Toray two different membranes were used to evaluate the possible difference between two of the same membranes. The one missing data point for the Toray and Hydranautics was due to limitations or problems experienced on the day of testing.

Table 3-2: Data collected from various experimental runs

Dates	Test	Concentrations (mg/L)						
		10	45	90	350	900	1400	2300
2021/09/15 and 2021/09/16 and 2021/09/17	Filmtec™ Permeability data (Membrane 1)				<1			
2021/09/15 and 2021/09/16 and 2021/09/17	Filmtec™ Data Set 1 (Membrane 1)			x	x	x		
2021/10/06	Filmtec™ Data Set 2 (Membrane 1)	x	x			x		x
2021/10/07 and 2021/10/08	Toray Permeability data (Membrane 1)				<1			
2021/10/07 and 2021/10/08	Toray Data Set 1 (Membrane 1)	x	x	x	x	x	x	
2021/11/03 and 2021/11/04	Toray Data Set 2 (Membrane 2)	x	x	x	x	x	x	x
2021/10/20 and 2021/10/22 and 2021/11/03	Hydranautics Permeability data (Membrane 1)				<1			
2021/10/20 and 2021/10/22	Hydranautics Data Set 1 (Membrane 1)	x	x	x	x	x	x	x
2021/11/03	Hydranautics Data Set 2 (Membrane 1)	x		x	x	x	x	x

3.5 Conclusion

Chapter 3 provides an experimental design and methodology which allow for the measurement of the membrane performance in a controlled manner over the identified feed concentration range. The specific equations are now defined and incorporated into a calculation method that allows the experimental data to determine the membrane-specific properties (constants). The rig was not temperature controlled and therefore the experimental points were used to obtain model parameters for the specific membrane. Using the model, the membrane performance could then be used to predict its behaviour if one process condition (e.g., temperature) was varied. Therefore, this chapter also detailed the methodology to model the membrane performance from the determined specific properties and operational parameters.

CHAPTER 4 RESULTS AND DISCUSSION

The data collected from the experimental work (Table 3-2) is analysed and discussed starting with the salt rejection and water flux results in Section 4.1. Section 4.2 presents the membrane-specific properties (membrane constants) that were derived from the experimental data and the values are compared to literature. The experimental data is compared to the modelled values with the obtained constants and discussed in Section 4.3. In Section 4.4 the model response to a change in a single parameter is evaluated and compared to relevant membrane literature.

As discussed in Chapter 3, the feed water temperature could not be controlled in the experimental setup which caused significant variance in the experimental conditions. This complicates the comparison and discussion of the experimental results. However, each single data point could be used for modelling purposes and from the model more meaningful correlations between membrane performance and operational parameters could be drawn, given in Sections 4.3, 4.4 and 4.5.

4.1 Experimental results

From the data collected for the three membranes given in Table 3-2 the observable performance of the membranes was evaluated. Two critical performance indicators, salt rejection and water flux were used as the main criteria.

4.1.1 Salt rejection

In Figure 4-1 the observed salt rejection calculated according to Equation 2-5 is plotted against the feed concentration.

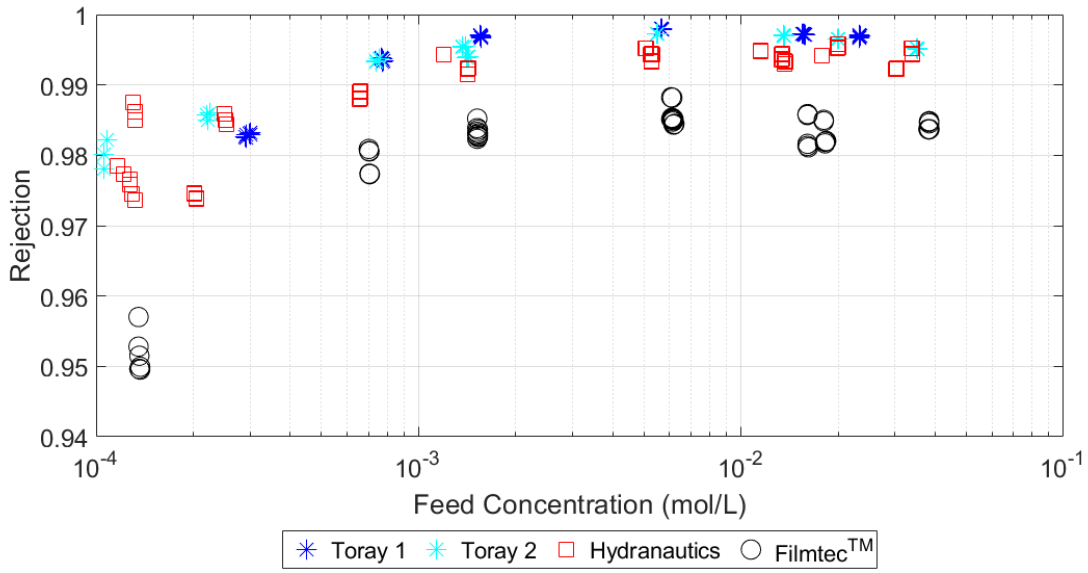

Figure 4-1: Experimental results for observed rejection compared to feed water concentration; Toray 1 and 2, Hydranautics and Filmtech™

Figure 4-1 indicates that all 3 membranes show the same trend with a significant reduction in salt rejection as the feed concentration reduces. A similar trend is observed for the reference plant (Figure 1-2) and by Bartels *et al.* (2005). For the feed concentrations above 100 mg/L both the Hydranautics and Filmtec™ membranes showed a constant salt rejection however, the Toray showed a clear peak at 500 mg/L and then started reducing as the feed concentration increased.

Comparing the salt rejection of the different membranes, the Filmtec™ membrane salt rejection is significantly lower than the other two. The Toray rejection was higher than the Hydranautics for all feed concentrations except the highest concentration where both membrane's rejection were similar. Toray 1 membrane salt rejection is slightly higher compared to Toray 2 for feed concentrations higher than 7.5×10^{-4} mol/L (43 mg/L).

In terms of the minimum salt rejection according to the supplier data sheets given in Table 3-1, the Toray membrane achieved 99.65% salt rejection. Hydranautics achieved a 99.4% salt rejection compared to the stated 99.8%. The Filmtec™ only reached 98.4% which is significantly lower than the datasheet reference of 99.5%. It must also be considered that the data sheet results given were taken at 25 ºC and exactly 15% recovery, which the experimental data did not duplicate. This can explain the difference in actual versus stated salt rejection.

4.1.2 Water permeability coefficient

The second parameter to evaluate the experimental results is the solvent flux or water flux. Utilising the data collected with feed water salt concentrations less than 1 µS/cm (demineralised water) the water permeability coefficient for each membrane was determined with the results displayed in Table 4-1. The first Toray membrane (Toray 1) was extensively tested with demineralised water at various temperatures to determine the temperature dependence of the water permeability coefficient. For the second membrane (Toray 2) the low feed concentrations were used to determine the permeability coefficient (L_{p25}) and the alpha value (α_{Lp}) was assumed to be the same as the first Toray membrane tested.

Table 4-1: Results of the constants determined for water permeability for each membrane

	Water Permeability (L/m^2.bar.h)			
	Toray 1	**Toray 2**	**Filmtec^{TM}**	**Hydranautics**
L_{p25}	4.7	4.0	3.3	3.6
α_{Lp}	0.044	0.044	0.043	0.037

The results from the modelling produced satisfying results for all the membranes and graphically shown in Figure 4-2.

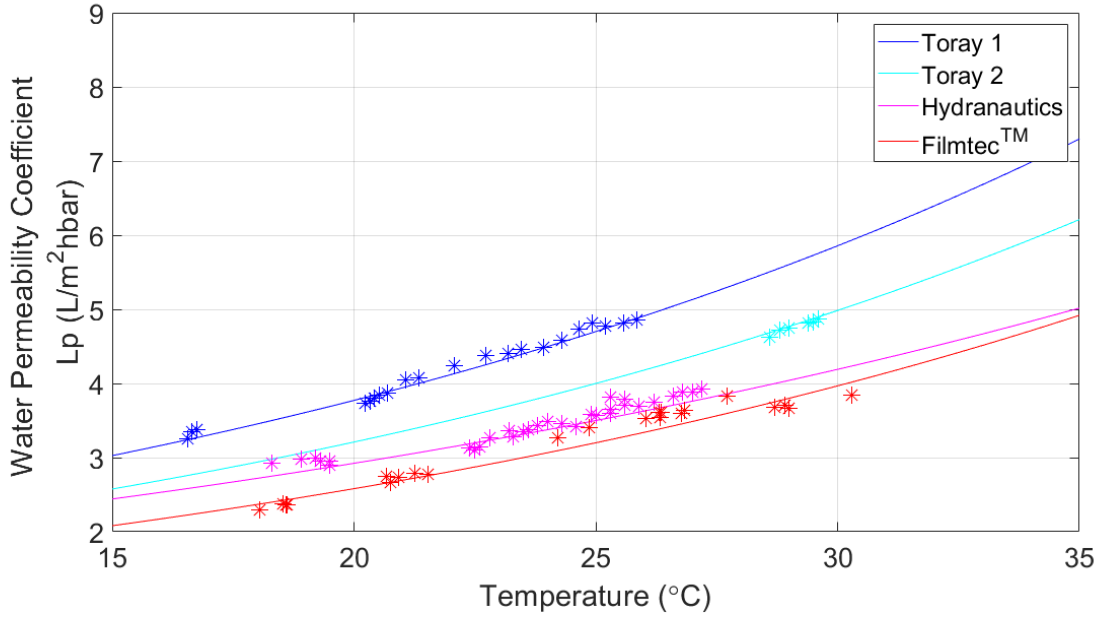

Figure 4-2: Comparing the three membranes water permeability curves versus temperature.

Figure 4-2 shows that both the Toray membranes have a higher water permeability than the other two membranes, followed by the Hydranautics and Filmtec™ membranes. However, there is a significant difference in permeability from Toray 1 to Toray 2 membrane. The data shown in Table 4-2 is a comparison of the water permeability results from this study and other studies at 25 ºC. The water permeability results from this study were generally higher than older studies and similar permeabilities were reported in recent studies by Alsarayreh, *et al.* (2021) and Li (2012). This is most likely due to the progress of RO technology to deliver a more economical and better-performing membrane.

Table 4-2: Other study's water permeability results at 25 ºC.

Study	Water Permeability at 25 ^{o}C			
	Membrane supplier	**Type of Membrane**	**Membrane Model**	**Lp (L/m^{2}hbar)**
This study	Toray	Brackish Water Membrane	TM700D	4.0 - 4.7
	Filmtec™	Brackish Water Membrane	BW30 - 4040	3.3
	Hydranautics	Brackish Water Membrane	CPA7-LD 4040	3.6
Li, 2019[1]	Filmtec™	Saltwater Membrane	30 SW 2.5"	1.17
Li, 2012	Unknown	Brackish Water Membrane	-	2.71
Taniguchi, *et al.*, 2001	Toray	Saltwater Membrane	UTC-80	0.91
Alsarayreh, *et al.*, 2021[2]	Toray	Brackish Water Membrane	TMG20D-400	3.46
	Filmtec™	Brackish Water Membrane	BW30-400	2.74
	Filmtec™	Brackish Water Membrane	BW30LE-440	4.37
	Toray	Brackish Water Membrane	Toray SU-820	4.09

4.2 Determining model constants

Using the experimental data collected with the model calculation detailed in paragraph 3.3 the reject pressure drop, water permeability, mass transfer coefficient, and salt flux constants were determined for each membrane.

[1] Although the study was done in 2019 the results were generated by another author (Avlonitis) in 1991.
[2] The data shown were collect by Alsarayreh *et al.* (2021) from other studies.

4.2.1 Reject pressure difference calculation

Experimental pressure difference data for each membrane were used as input for the optimisation calculations in MATLAB® to determine the constants b_r and m_r from Equation 3-1.

Table 4-3: Results for the constants to be calculated for the pressure difference over the feed to the reject of the membranes

	Pressure difference data outputs		
	Toray	**Filmtec™**	**Hydranautics**
br	3.3×10^{-6}	1.2×10^{-5}	1.1×10^{-5}
mr	0.19	0.18	0.18

The modelled results were satisfactory with all 3 membranes comparison between modelled and actual data and the results are graphically shown in Figure 4-3. The reject pressure difference is used in the model to determine the average pressure applied across the membrane and used in determining the permeability characteristics and the permeate flow. Li (2012) determined a m_r value of 0.18 for the data collected on a spiral wound seawater membrane, similar to the results in Table 4-3.

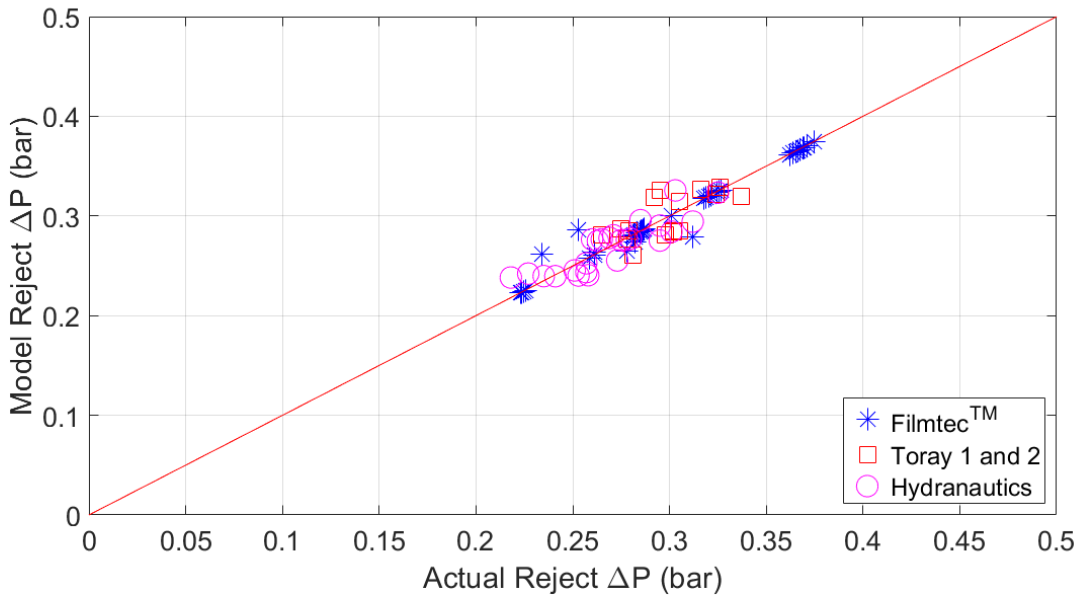

Figure 4-3: Reject pressure difference comparison between actual measurements and modelled data for the three different membranes.

4.2.2 Salt permeability coefficient

The salt permeability constants B_{s25} and α_B are determined using several other constants (b_m, β, γ, b_1 , FF and K) using the calculation sequence described in Section 3.3.4. The salt permeability results for each membrane are shown in Table 4-4 and Figure 4-4.

Table 4-4: Salt permeability constants determined from experimental data for each membrane.

	Salt Permeability (L/m^{2}h)			
	Toray 1	**Toray 2**	**Filmtec™**	**Hydranautics**
B_{s25}	0.0012	0.038	0.24	0.070
α_B	1.9x10^{-1}	1.9x10^{-2}	1.5x10^{-5}	1.2x10^{-2}

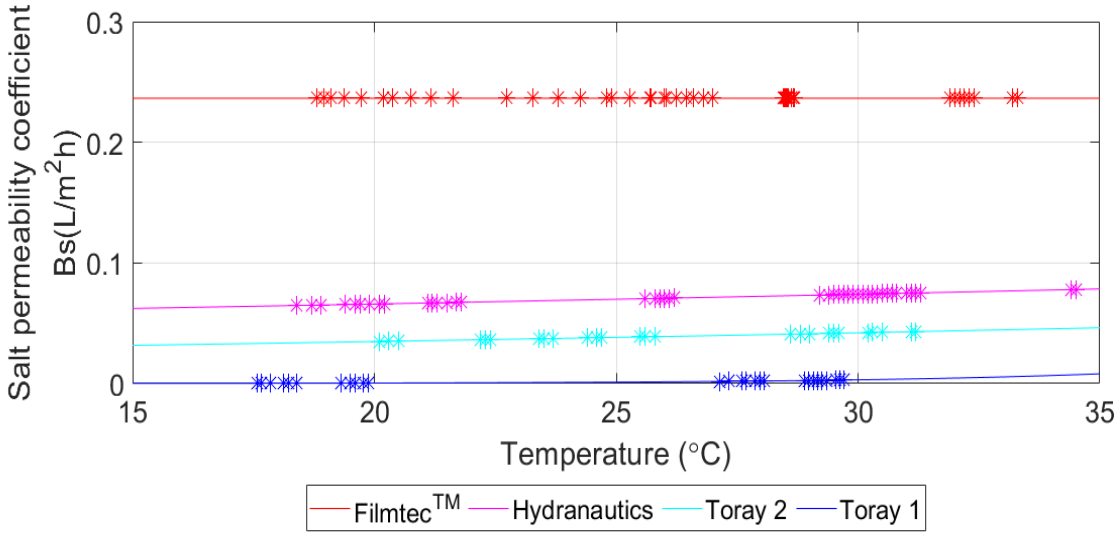

Figure 4-4: Salt permeability curves for each membrane against temperature.

The salt permeability for Filmtec™ is significantly higher compared to the other membranes, with Toray 1 showing the lowest value. Higher salt permeability will result in lower salt rejection (DuPont, 2016), referring to the observed rejection results shown in Figure 4-1, a correlation can be seen although the observed rejection is not temperature corrected as the permeability presented in Figure 4-4. The expectation from Equation 3-9 is that the salt permeability will increase exponentially with temperature. The greater the value of α_B the higher the temperature dependence, all three membranes showed a low dependence on temperature for the salt permeability seen in the low values of α_B in Table 4-4 and the almost flat lines in Figure 4-4.

The Filmtec™ membrane has a significantly higher salt permeability compared to the other two membranes. The salt permeability difference between the two Toray membranes is also significant.

Table 4-5: Comparison of Salt permeability at 25 ºC from other studies.

Study	Salt Permeability at 25 °C			
	Membrane supplier	Type of Membrane	Membrane Model	Bs (L/m²h)
This study	Toray	Brackish Water Membrane	TM700D	0.001 – 0.038
	Filmtec™	Brackish Water Membrane	BW30 - 4040	0.237
	Hydranautics	Brackish Water Membrane	CPA7-LD 4040	0.070
Li, 2019	Filmtec™	Saltwater Membrane	30 SW 2.5"	0.14
Mickols 2019[3]	Filmtec™	Brackish Water Membrane	BW30XFR	0.3 - 0.7
Alsarayreh, *et al.*, 2021[4]	Toray	Brackish Water Membrane	TMG20D-400	0.58
	Filmtec™	Brackish Water Membrane	BW30-400	0.22
	Filmtec™	Brackish Water Membrane	BW30LE-440	0.09
	Toray	Brackish Water Membrane	Toray SU-820	0.82

Table 4-5 shows the results of the salt permeability at 25 ºC compared to other studies. In comparison all three membranes' salt permeability is much lower than in other studies, even the Filmtec™ results were low compared to the other studies. The Hydranautics showed at least 1 order lower salt permeability values and the Toray membrane was 1 order lower than the lowest of any other study.

4.2.3 Mass transfer coefficient

The constant b_m for Equation 3-6 and two coefficients β and γ for the Deissler equation (Equation 2-10), b_1 and K were also determined for each membrane. Equation 3-6 could then be solved to determine the concentration at the membrane wall ($\bar{c}_m$). Once the membrane wall concentration is known the concentration polarisation (CP) and therefore the mass transfer coefficient (k) could be determined for each membrane.

[3] Mickols (2019) varied flux of the membrane at constant temperature of 25 ºC.
[4] The data shown were collect by Alsarayreh *et al.* (2021) from other studies.

Once the mass transfer coefficient for the experimental data was determined, the last constant (α) of the Deissler equation is determined. The final values of the constants for each membrane tested are shown in Table 4-6.

Table 4-6: Calculated constants determined for each membrane

	Mass transfer modelling			
	Toray 1	**Toray 2**	**Filmtec™**	**Hydranautics**
α	0.39	0.067	0.094	0.11
β	0.0041	0.0011	0.0015	0.021
γ	0.81	0.81	0.81	0.81
b_m	7.1×10^{-4}	7.1×10^{-2}	3.6×10^{-2}	2.7×10^{-3}
b_1	7.5×10^{-3}	2.0×10^{-7}	6.2×10^{-6}	1.5×10^{-3}
K	1.9×10^{-4}	1.0×10^{-4}	2.6×10^{-4}	1.1×10^{-4}

Other studies', shown in Table 2-1, determined values for α between 0.0096 and 0.2 with the calculated values for the four membranes in this range. For β the other studies' range is between 0.5 and 0.875 and for γ between 0.25 and 0.6. The results in Table 4-6 are much lower for β compared to the other studies and higher for γ. Although the values for β and γ vary significantly from the other studies, the values for the four tested membranes were very similar. The Deissler equation allows for these constants to vary to provide a practical representation of the mass transfer for the application, which was achieved for the four membranes.

Anisimov & Orlov (2018) determined the K value for their tested seawater membrane and NaCl, the only other study with this constant, to be 6.75×10^{-6} and the values for the membranes in this study varied between 1.05 – 2.55×10^{-4} which is 2 orders of difference. Anisimov & Orlov (2018) results were reported on a seawater RO membrane compared to the brackish water RO membranes tested in this study. Since the K value is representative of the molar flux of the ions and therefore dependent on the membrane-specific characteristic the difference can be contributed to the difference between the two types of membranes.

4.3 Modelling of NaCl experimental data

Using the actual experimental feed data for concentration, pressure, flow rate, temperature and permeate pressure as input into the model the permeate flow and permeate quality are determined for all 3 membranes for all experimental measurements. The output of the model is then evaluated in terms of permeate flow and permeate quality compared to the measured values.

The modelled data are all graphically presented as single points because the experiment temperature was not controlled. Therefore, more than one variable is changing between different data points used as input for the model calculation

4.3.1 Modelling permeate flow

When the model results are evaluated without taking into consideration the deliberate fouling (FF = 1) that was done for the Filmtec™ and Hydranautics membrane a clear offset in the permeate flow model results is observed. These data points were parallel to the parity line with a constant offset as presented in Figure 4-5 for the Filmtec™ permeate flow data. The fresh membranes permeate flow was very well predicted.

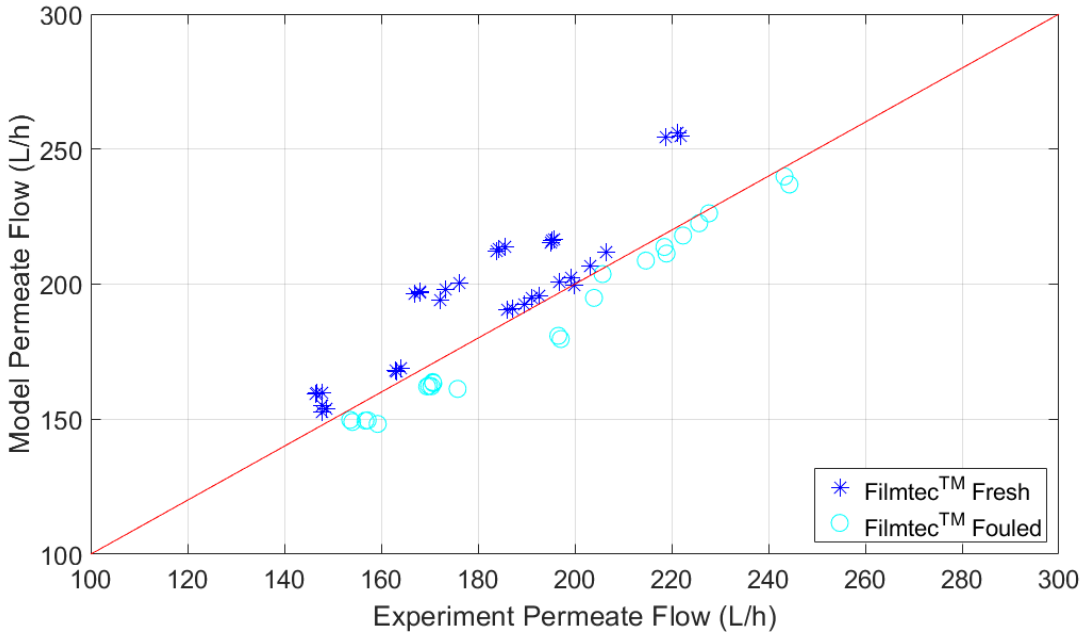

Figure 4-5: Filmtec™ permeate flow experimental vs model data without fouling factor showing offset in data.

With the deliberate fouling that was done for the Hydranautics and Filmtec™ membranes a lower permeate flow will be expected for the same operating conditions. The lower flow values to the parity line in Figure 4-5 is expected therefore, the fouling factor given in Equation 3-8 must be used.For the first data set for each membrane, a fouling factor of 1 was allocated to all data points collected. For the second data set, a fixed fouling factor was provided for all the data points in that data set according to Table 4-7.

Table 4-7: Fouling factors assigned to each data set collected.

Dates	Test	Fouling Factor
2021/09/15 and 2021/09/16 and 2021/09/17	Filmtec™ Data Set 1 (Membrane 1)	1
2021/10/06	Filmtec™ Data Set 2 (Membrane 1)	0.9
2021/10/07 and 2021/10/08	Toray Data Set 1 (Membrane 1)	1
2021/11/03 and 2021/11/04	Toray Data Set 2 (Membrane 2)	1
2021/10/20 and 2021/10/22	Hydranautics Data Set 1 (Membrane 1)	1
2021/11/03	Hydranautics Data Set 2 (Membrane 1)	0.95

The permeate flow results from the model calculation with the fouling factors are plotted against the measured permeate flow with a parity line in Figure 4-6.

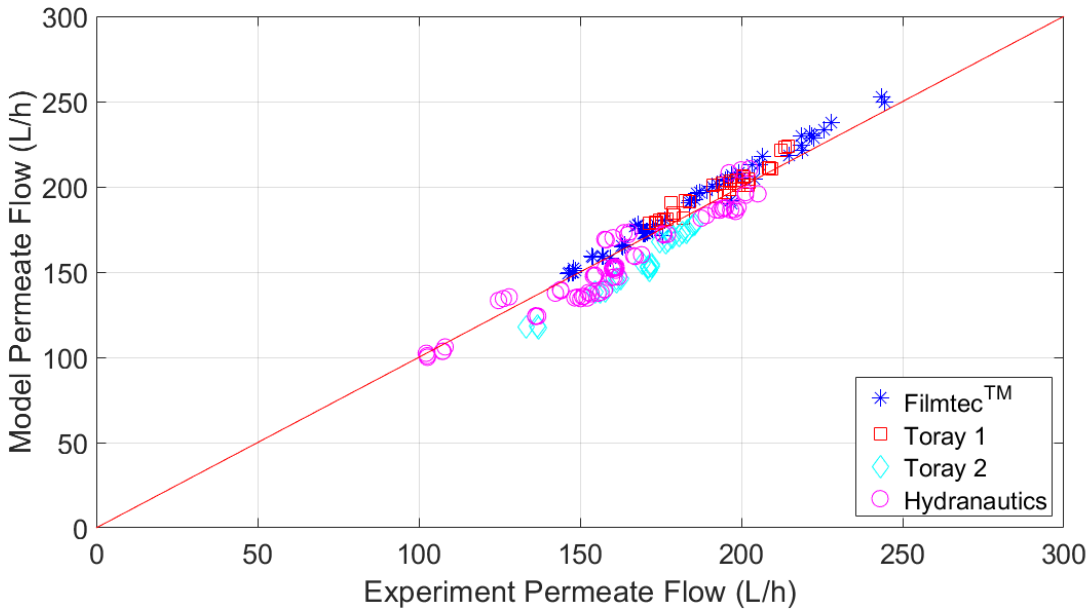

Figure 4-6: Experimental permeate flow compared to modelled permeate flow.

The permeate flow calculated by the model for all the membranes with good linear regression values (R^2) for Filmtec™ at 0.98, Toray 1 at 0.93, Toray 2 at 0.90 and Hydranautics at 0.91. The results confirm that the model can predict the permeate flow rate accurately.

4.3.2 Modelling permeate quality

The second result required from the modelling is the permeate quality to calculate the salt rejection. The experimental salt rejection data presented earlier in Figure 4-1 showed a definite change in the trend at feed concentrations below 100 mg/L (1.7x10^{-3} mol/L). Solving with the standard salt flux equation (Equation 2-4) the model did not predict the permeate concentration below this pivot point in the data, these results are represented as the *Standard model* in Figure 4-7. The *Modified model* includes two additional terms for the convective salt transport ($J_{si}{}^{K}$) and additional term ($J_{si}{}^{F}$) as given in Equation 3-7. To demonstrate the difference between the Standard and Modified model only one set of data (Hydranautics) is compared with the experimental results in Figure 4-7.

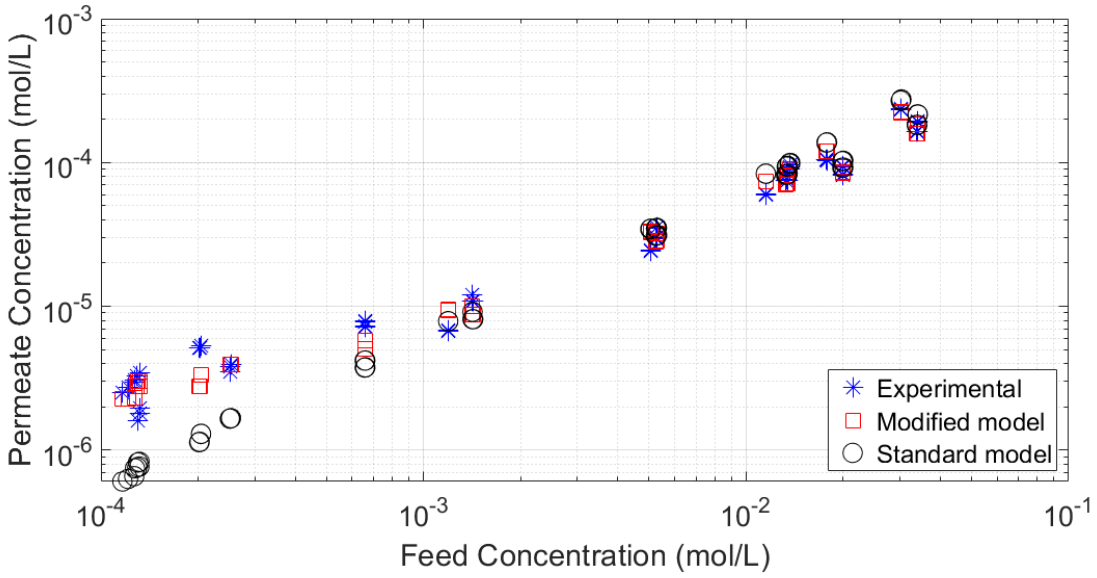

Figure 4-7: Experimental permeate concentrations versus the standard model and modified model for the Hydranautics data sets.

The standard model predicted an almost straight line to the zero point and therefore produced much lower permeate concentrations than the measured experimental values. In a study done by Galama *et al.* (2013) a straight line through zero was expected when they included the Donnan effect on cation and anion-charged RO membranes instead, they found a similar change in the experimental data as the feed concentration decreases.

The standard model is not fit for purpose therefore, the modified model is selected as the preferred model and is applied to the experimental conditions for all four membranes. The result from the modified model is compared to the measured experimental results in terms of permeate concentration in Figure 4-8 and salt rejection in Figure 4-9.

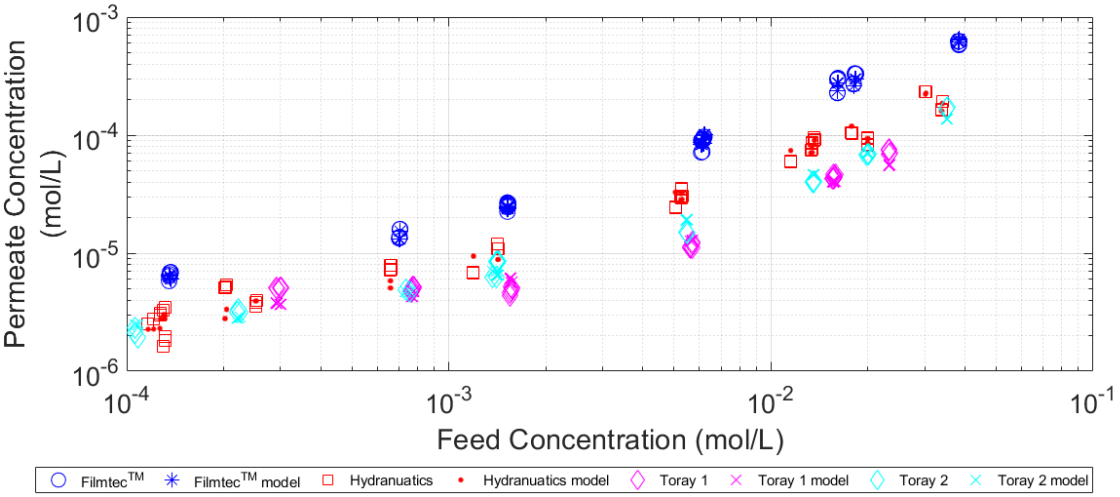

Figure 4-8: Experimental permeate concentration against modelled concentration

The results presented in Figure 4-8 for the permeate quality produced a good data fit according to the regression analysis for the membranes with R^2 values of 0.994 for Filmtec™, 0.947 for Toray 1, 0.901 for Toray 2 and 0.992 for Hydranautics. The model results correspond very well with the experimental results for all three membranes across the whole feed concentration range. The trend shows that the permeate concentration is not in a linear relationship to the feed concentration with a definite change in slope at around $1x10^{-3}$ mol/L (60 mg/L) for all three membranes, more clearly for Toray and Hydranautics than Filmtec™ membranes than the Filmtec™ membrane. Similar observations were made by Anisimov & Orlov (2018) and Galama *et al.* (2013) who attributed this decrease in rejection to the decrease in the Donnan effect.

With the permeate concentrations accurately determined by the model the observed rejection is also modelled with good accuracy and is visually presented in Figure 4-9. The modified model's ability to accurately predict the membrane permeate concentration throughout the whole feed concentration range is significant for two reasons. Firstly, the results confirm the validity of the Anisimov & Orlov (2018) additions to the solute flux equation. Secondly, the results confirm that the Donnan effect reduction is the cause of the lower rejection at lower feed concentrations.

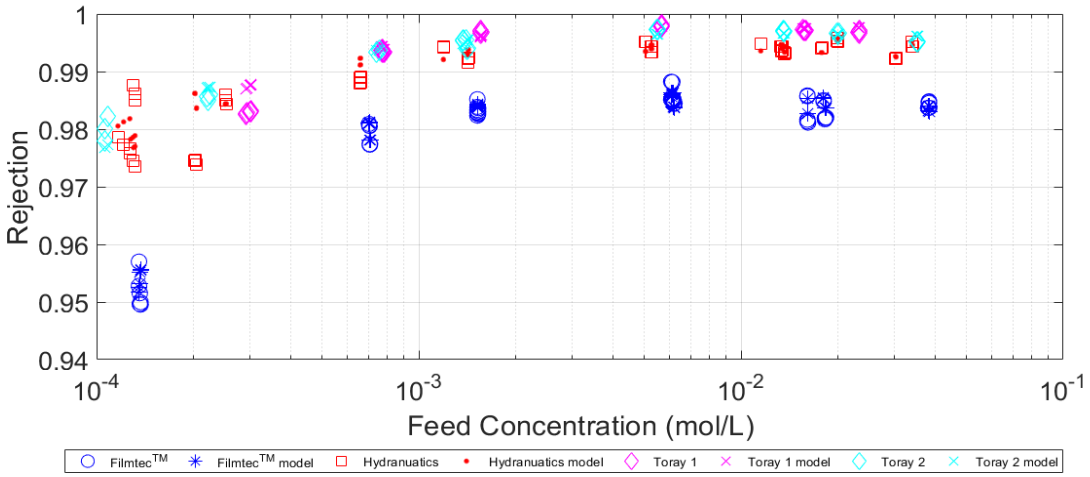

Figure 4-9: Experimental rejection versus model rejection.

4.4 Validating model response

After evaluating the model results to the NaCl experimental data the model is further tested in terms of its response according to the expected performance for RO membranes for given changes in feed pressure, temperature, and concentration (Figure 2-1). The membrane constants determined from the experimental measurements in Section 4.2 are implemented in the model calculation method as described in Section 3.3.5. Since the trends for the three membranes are very similar, only one set of constants (Hydranautics) is shown.

The feed concentration, feed pressure and feed temperature were selected as variables for the validation with the input parameters to the model being feed pressure, feed flow rate, temperature, concentration and permeate pressure. For the first scenario, only the feed concentration was changed, and all other input parameters were fixed. For the second case, only the feed pressure was changed between 5 to 15 bar. The third case only changed the temperature between 15 and 35 ºC.

The results for the variation in feed concentrations are presented in Figure 4-10.

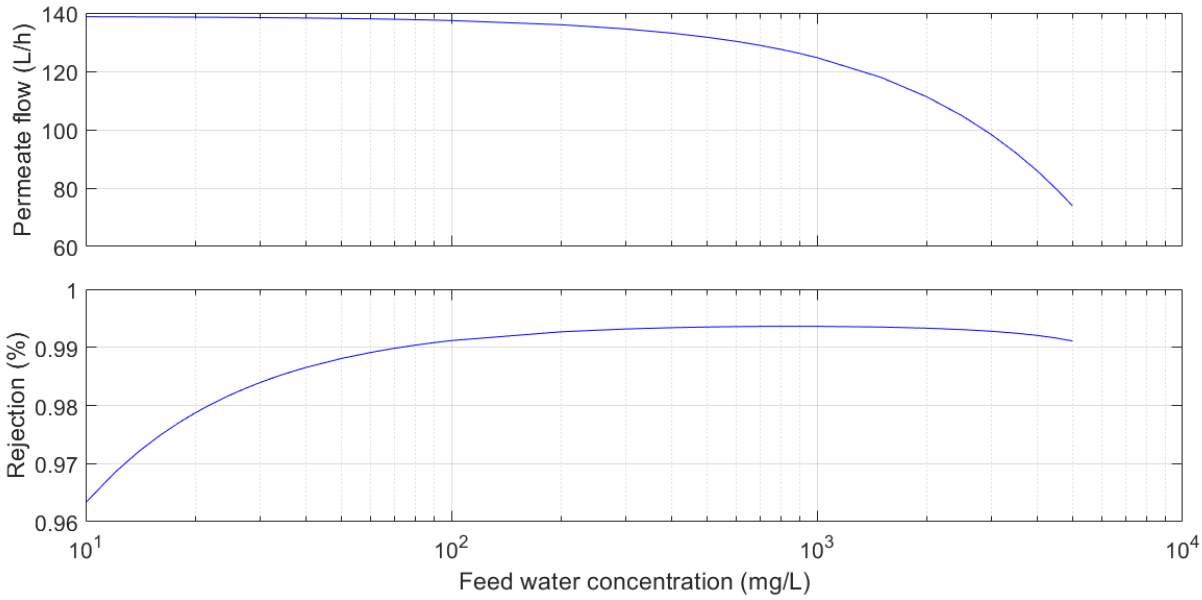

Figure 4-10: Model verification with varying feed water concentration and constant feed pressure, feed flow and temperature.

The permeate flow decreases with increased feed water concentration. Referring to Equation 2-1 the increase in osmotic pressure and constant feed pressure reduces the net driving pressure and therefore the permeate flow will decrease with an increase in feed concentration. (Abdulsalam Ebrahim *et al.*, 2020; Chen & Qin, 2019; DuPont, 2019)

The salt rejection increase as feed water concentration reaches an optimum point at 1000 mg/L and then starts to slowly decrease as the feed concentration further increases. The result is consistent with the predicted curves shown in Figure 2-1 and Figure 2-2. Other studies showed that the Donnan effect is dependent on the feed concentration, the influence of the effect is most dominant in the 500 to 2000 mg/L region. Above and below this optimum feed concentration range the influence of the Donnan effect decreases leading to a decrease in salt rejection. (Anisimov & Orlov, 2018; Bartels *et al.*, 2005; Ebrahim *et al.*, 2020)

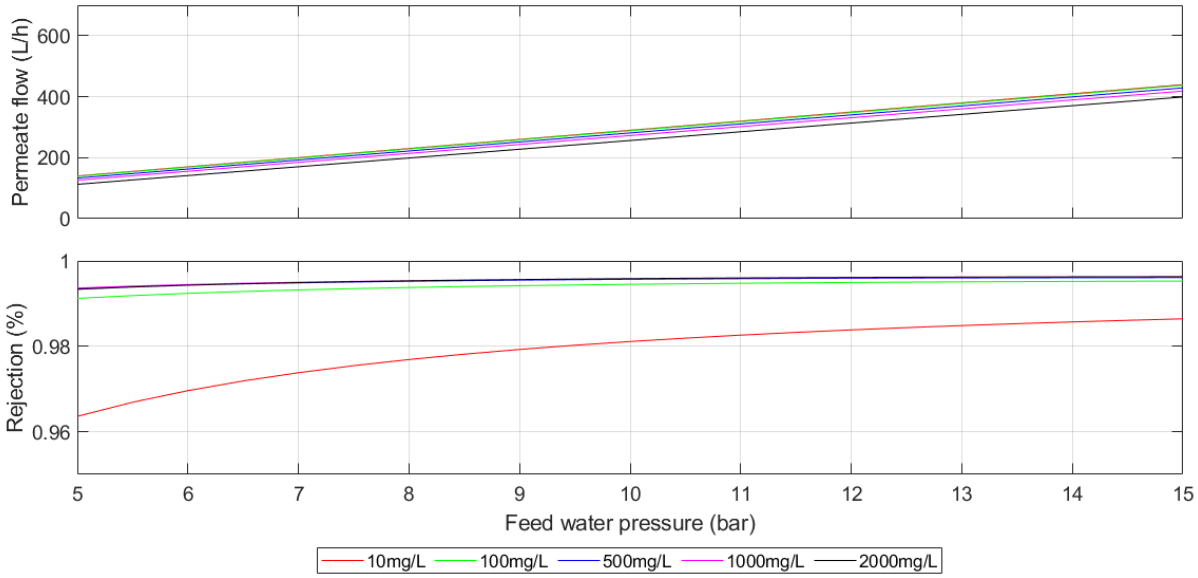

Figure 4-11: Model verification with different feed concentrations and feed water pressure at constant feed flow and temperature.

The model results for changing the feed water pressure at various feed concentrations are given in Figure 4-11. The model predicts a linear relationship with increasing permeate flow at increasing feed pressure for all feed concentrations. The equation for permeate flux (2-1) shows that the permeate flow is directly proportional to the pressure difference over the membrane therefore, the increase in feed pressure will increase the permeate flow.

The salt rejection shows an increase in rejection and then reaches an optimum as the feed pressure further increases. The salt flux, represented by Equation 2-4 in its simplest form, is independent of the pressure difference and therefore independent of the permeate flow. As the permeate flow increases with a constant salt flux the permeate concentration will decrease and the salt rejection will increase. (DuPont, 2019; Hung *et al.*, 2011; Jang *et al.*, 2019; Maddah & Almugahwi, 2017; Mickols *et al.*, 2021)

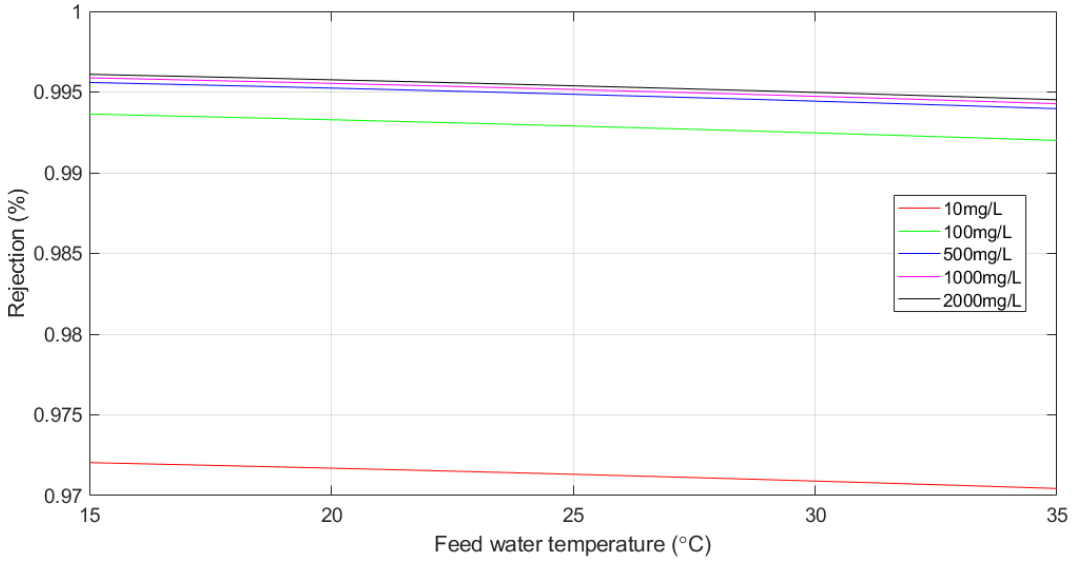

Figure 4-12: Model verification at different feed concentrations with varying feed water temperatures at constant flux, feed pressure and feed flow.

The feed temperature was varied at different feed concentrations with constant flux. To fix the flux recovery of 15% was used as input therefore, the permeate flow was constant at 180 L/h. The salt rejection decreased with increased temperature, the membrane solute flux increases with an increase in temperature (Equation 2-17) therefore it is expected that the salt rejection will decrease. (Alsarayreh *et al.*, 2021; Jin *et al.*, 2009; Shen *et al.*, 2016)

For all three variations, the results predicted by the modelling fit with the expected response as predicted by the model equation and literature review. The validation of the model, therefore, confirms that the model can predict the membrane performance throughout the operating range and that the obtained constants for the different membranes can be compared on equal footing.

4.5 Conclusion on experimental results and modelling

The salt and water permeability constants for the Filmtec™ membrane showed significantly higher salt permeability and lower water permeability values compared to the other two suppliers' membranes. Between the Toray and Hydranautics membranes, the Toray membranes produced slightly better (lower) salt permeability capabilities with higher water permeabilities compared to the Hydranautics membrane. Therefore, the Toray membrane showed to be the most efficient in terms of salt and water permeability for the different membranes tested which makes it the preferred membrane under the tested conditions.

The difference in water permeability between the two Toray membranes was not expected, since both membranes were procured together from the same supplier at the same time. The membranes were prepared for the experimental work using similar flushing techniques and operated in similar operating conditions. The only conclusion is that the variability could be caused by the manufacturing, storing and transporting of the membranes which could affect the performance of the membrane, no studies investigating this aspect were found in more detail.

The offset in the permeate flow data caused by the induced fouling is clearly shown in the model results, thereby confirming that the deliberate fouling did manage to make a significant difference in the membrane's water permeabilities. The fouling however did not impact the salt permeability of the fouled membrane. The fouling factor incorporated into the model is effective in predicting the permeate flow of aged membranes.

Using the experimental data, the membranes could well be characterised with the constants required in the model equations, the constants also conformed well to RO membrane's behaviour compared to other studies' results. The model developed can predict accurate permeate flow and quality results for all three membranes. Significantly, the modelling success agreement of the permeate quality at feed concentrations below 100 mg/L is due to the modified solute flux equation used in the model. Accounting for the Donnan effect and being able to model its effect accurately demonstrated the impact of the Donnan effect and explains the reduction in salt rejection at lower feed concentrations.

CHAPTER 5 REFERENCE PLANT OPTIMISATION

In designing an RO system, three important goals must be reached: maximum product quantity and quality and minimum waste quantity. The quantity of the product (permeate) and waste (reject) streams are determined by the recovery of the RO system and the product quality by the salt rejection. To achieve the desired salt rejection, the correct membranes must be selected for the application and then operated within its design limits, such as temperature, pH, pressure difference, particulate solids loading, minimum flow rates and recoveries. The system recovery is dependent on the salt rejection since the reject water concentration increases after each membrane and the reject can only be concentrated to certain limits. The configuration of the plant also plays a role, by configuring the vessels in different passes and stages (refer to Appendix A) the plant production and overall recovery can be optimised to produce the most economical solution to reach the target quantities and quality. (DuPont, 2016)

The experimental work described in Chapter 3 with the results presented in Chapter 4 showed that the observed reduction in rejection with low feed concentrations can be attributed to the change in the Donnan effect. This answered the initial question of why the salt rejection reduces with feed concentration and since the Donnan and hence the reduced rejection cannot be directly controlled with the current available RO membrane technology. Therefore, with no means to increase the salt rejection at lower feed concentrations, the only optimisation measure available is to increase the water recovery to the maximum possible values.

Complex configuration designs such as the reference plant consisting of RO Pass 1 (with 3 stages) and RO Pass 2 (with 2 stages) with various recycle streams make the modelling very challenging, especially if required to be built from first principles. Software modelling tools assist greatly in reducing calculation time and effort by removing the requirement to go through all the equations, properties, limits, and iterations. The water treatment plant industry does not have common design software packages which incorporate different suppliers' information in one central tool. Since the performance of each membrane model and supplier is unique, the software packages require typical experimental data, similar to what is presented in Chapters 3 and 4, to model the membrane. This information is generally only known by the supplier and it is seen as their intellectual property (IP). This has led to each supplier developing its design tool for its technology which might not be limited to RO membranes only but can also include ion exchange (IX), nano-filtration (NF) and ultrafiltration (UF). The software is normally free to use and can be downloaded from the suppliers' websites with the required instructions to operate it, the software is user-friendly and can be used without extensive training.

The model developed in Chapters 3 and 4 is not refined enough to model a complex configuration as the reference plant and can therefore not be used to complete the optimisation. The OEM software also has the advantage that it already contains the membrane limits i.e., maximum recovery, minimum and maximum reject and permeate flow etc. The software thereby assists the user by displaying alarms when the limits are exceeded for any membrane in the system to ensure the design is correctly done. The software has the added benefit that can easily model several cases with different configurations and operating conditions and can then be used to compare the results to select the optimum solution.

5.1 OEM Modelling software

Each of the suppliers' membranes used in this study has its own modelling software. To compare the software results with the experimental work and the developed model the experimental operating conditions for each membrane data were entered into the software. The OEM software was set up based on the experimental permeate flow, recovery, feed water temperature and feed water concentration for selected experimental data points over the entire feed concentration range. The results from the software modelling are compared to the experimental data and the developed model from Chapter 4. For the Filmtec™ membranes, the OEM developed WAVE™, version 1.82.824 with calculation engine 01.12.20.03 and database version 39 is used (DuPont, 2022). Toray membranes are modelled with Toray Design System 2.0©, version 2.3.1.205 with database version 2.8 and membrane database 20161 (Toray, 2022). Hydranautics membranes are modelled with Integrated Membrane Solutions Design (IMSDesign©), version 2.231.2107.09.90 (Hydranautics, 2022).

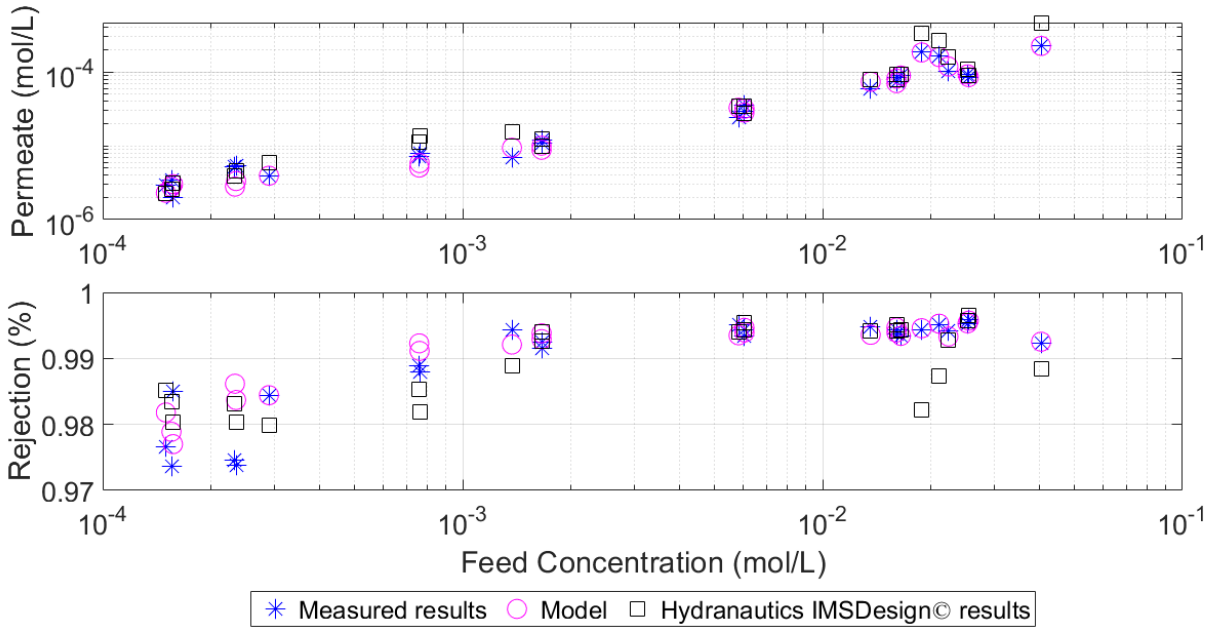

Figure 5-1: The Hydranautics IMSDesign© software results compared against experimental data and the model developed in this study.

The IMSDesign© software was able to predict the experimental permeate concentration very well except for a few data points at 7.5×10^{-4} mol/L (43 mg/L) and 2×10^{-2} mol/L (1150 mg/L). When investigating these data points, it was found that all of them were with a recovery of less than 13% therefore, operating at a much lower flux. In Section 4.4, where the model response is demonstrated, it is expected that salt rejection will decreases with lower flux however, it appears that the software predicts an even lower salt rejection at the low flux operating conditions compared to the experimental results.

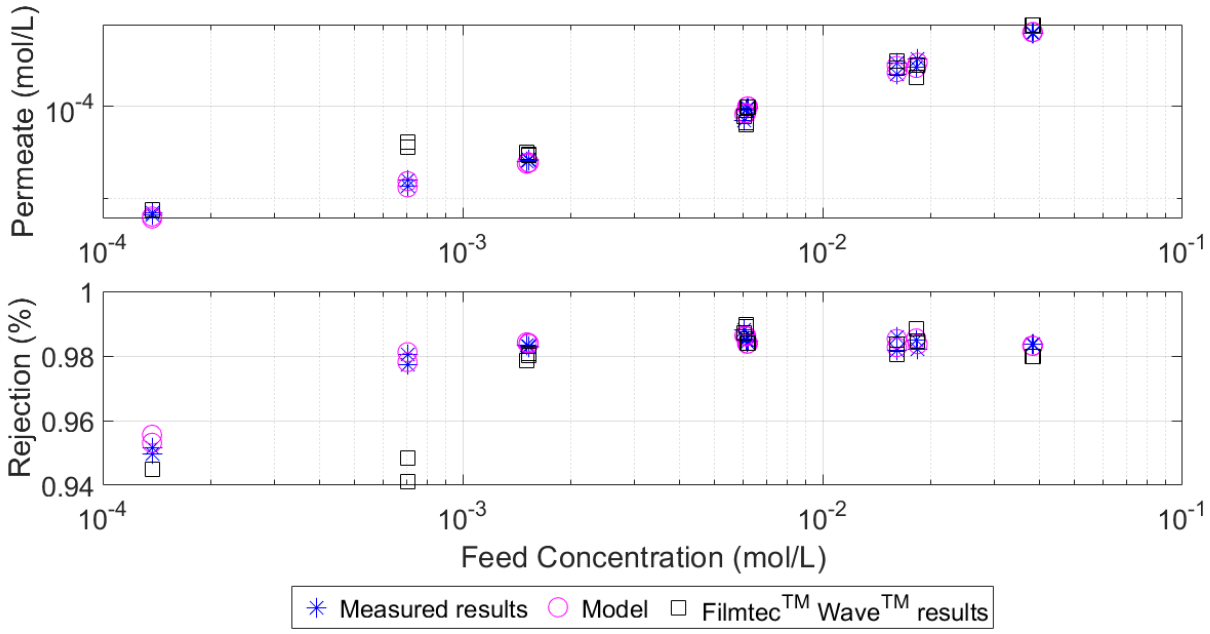

Figure 5-2: The Filmtec™ WAVE™ software results compared against experimental data and the model developed in this study.

The results from the WAVE™ software predicted the experimental results very well except for two data points at 7x10^{-4} mol/L (40 mg/L) feed concentration which was operated at feed water temperatures of 32 ºC. Keeping all input data the same in WAVE™ and only the changing temperature input to 25 ºC, WAVE™ predicted a better corresponding result compared to the measured values. It appears that the software expects a higher salt flux at the higher temperature which is why it predicts a lower salt rejection. WAVE™ may use a higher temperature dependence coefficient (α_B) compared to the experimental results.

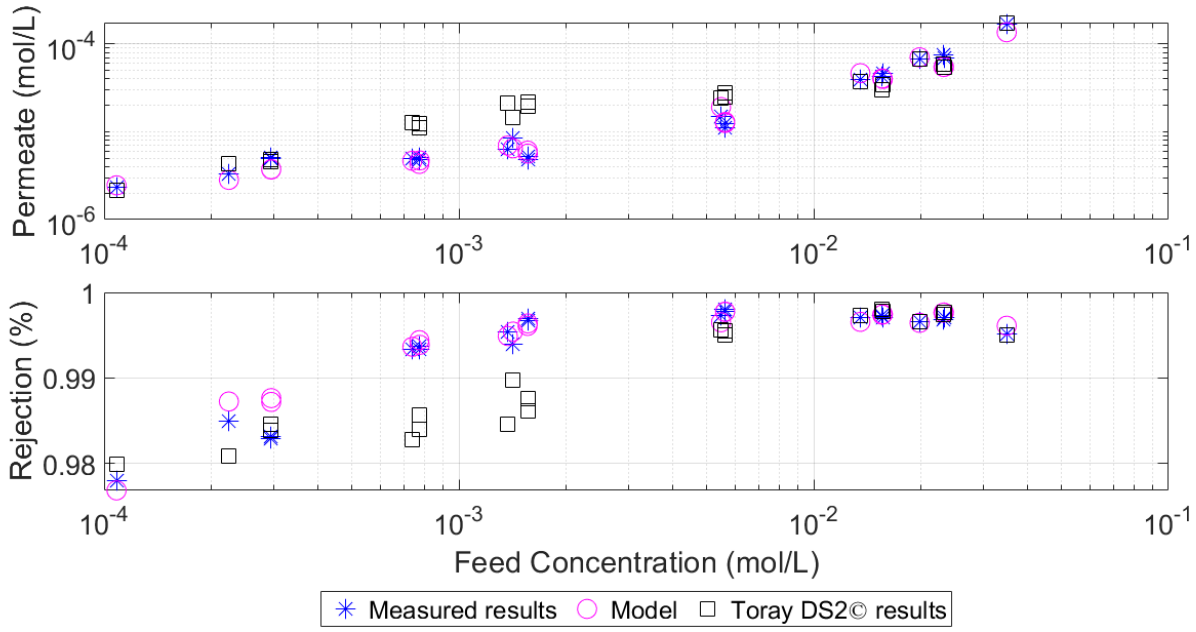

Figure 5-3: The Toray DS2© software results compared against experimental data and the model developed in this study.

The Toray DS2© software predicted the experimental results very well above 5.5x10^{-3} mol/L (320 mg/L) and below 3x10^{-4} mol/L (18 mg/L). In between these feed concentrations, the Toray predicts lower rejection compared to the experimental results. Following the pattern of the salt rejection, the software results expect the reduction in rejection to happen at a much higher feed concentration compared to the experimental results. It also appears to have two slope changes, a steep downward change at 4.5x10^{-3} mol/L (260 mg/L) and then the second slope change at 1.5x10^{-3} mol/L (90 mg/L) to a much flatter trend line. This is most likely due to the different correlation and modelling equations used in the software compared to the ones used in Chapter 3.

In general, all three software packages compared reasonably well with the experimental results. This provides the necessary confidence in the software packages to predict the plant performance therefore, it can be used in the optimisation of the reference plant. OEM software such as WAVE™, IMSDesign© and DS2© forms a critical part of the industry since this software is used extensively in the design and operational optimisation process for water treatment plants making the comparison important to provide confirmation in the software accuracy.

5.2 Optimisation of reference plant design

The optimisation exercise is done with the WAVE™ software using the Filmtec™ 8” BW30XFR-400 membrane although the Toray membrane tested as the best-performing membrane. The reference plant currently has Filmtec™ 8” BW30XFR-400 membranes installed therefore the optimisation was done according to the Fimtec™ membranes limitations and the original plant design was done with the Filmtec™ software.

According to the technical design manual, the factors influencing RO performance are, feed pressure, temperature, feed salt concentration, recovery and pH (DuPont, 2019). Feed pressure is a result of recovery, salt concentration, temperature, and membrane condition, therefore it is not available as a direct optimisation parameter. Temperature cannot be controlled in the reference plant and is therefore not used for optimisation. The influence of pH was not investigated in this study and therefore also no optimisation is recommended in terms of pH. Salt concentration cannot be directly controlled and is determined by the water mixture based on source water availability. Thus, only leaving recovery as an optimisation measure. In Figure 5-4 the optimisation of the reference plant is displayed; the details of RO 1 and RO 2 optimisation are given in Section 5.2.1 and 5.2.2.

5.2.1 RO Pass 1 optimisation

Based on the experimental membrane rejection performance over the feed concentration range there is a definite optimum feed concentration range between 500 – 2000 mg/L, a similar optimum range was also demonstrated by Anisimov & Orlov (2018) and Bartels, *et al.*(2005). The maximum theoretical recovery of an RO system is based on the potential for scale formation, determined by the feed water quality of the RO system (Byrne, 2002; Shahid & Choi, 2018). Should it be possible to increase the feed concentration and/or operate on the maximum recovery, the plant should be able to operate more efficiently with less reject and better permeate quality. Therefore, the solution is focused on operating RO Pass 1 on the limits of the feed water quality.

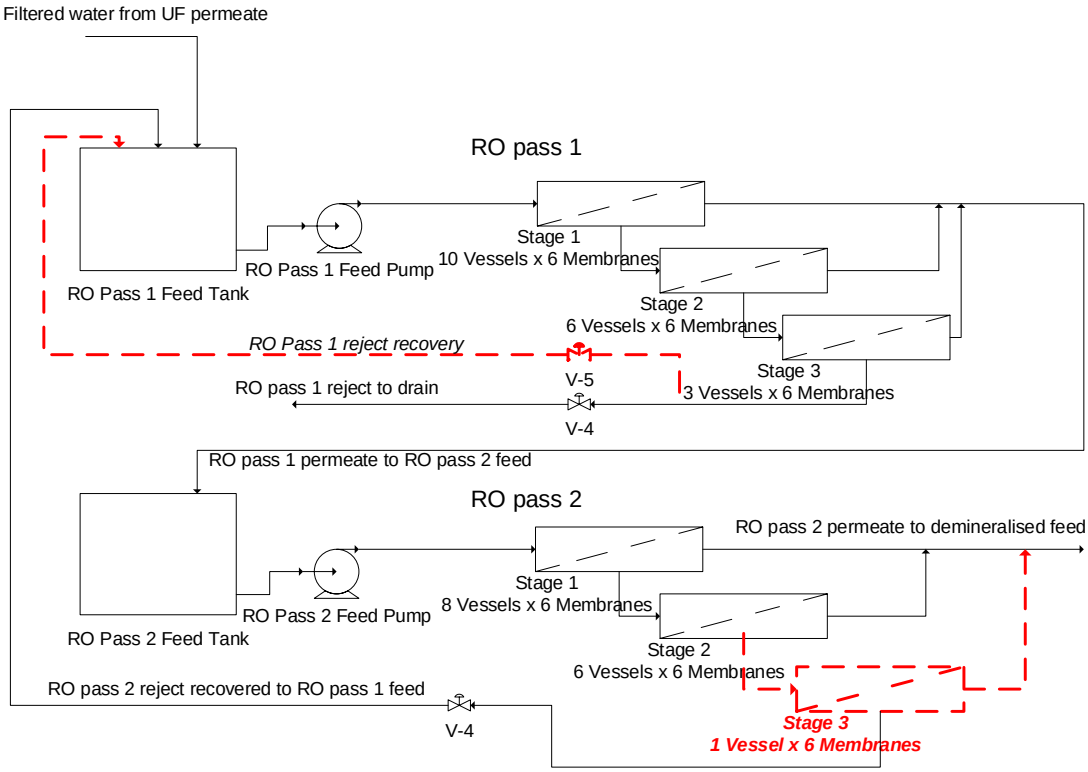

Figure 5-4: Recommended plant configuration changes (shown by ---) to increase water recovery and improve plant efficiency.

The recovery of each RO train is controlled by the reject flow control valve with an operating range determined by the membrane and its configuration. For the reference plant, the recovery is limited at 84% due to the flux limitations on stage 1 membranes (detailed plant configuration given in Appendix A). However, the maximum theoretical recovery of RO pass 1 is based on the potential for scale formation determined by the feed water quality as it concentrates up in the system (Byrne, 2002; Shahid & Choi, 2018). In a study done by Eskom and its chemical supplier for antiscalant the recovery limit for RO Pass 1, based on the design water qualities for Water A (Table 1-1) was found to be 97%, refer to Appendix D. To provide some margin on the scaling potential the target recovery was set at 96% for RO pass 1. (Eskom, 2018)

To further reach the target recovery, two options were evaluated. Firstly, increasing the number of membranes by adding vessels to the different stages of RO Pass 1. Secondly, a portion of the reject flow from RO Pass 1 can be recycled to the feed tank, thereby increasing overall recovery for RO Pass 1 without adding vessels or membranes to the plant.

Evaluating the current configuration for RO 1 to reach a 95% recovery by adding additional vessels will change from 22 vessels (Stage 1 – 12, Stage 2 – 6, Stage 3 – 4) to 32 vessels (Stage 1 – 19, Stage 2 – 7, Stage 3 – 4, Stage 4 – 2). The additional vessels and membranes are not only expensive but require significant modification in terms of arrangement and additional

pipework to accommodate auxiliary systems such as the Clean in Place (CIP). This arrangement will also not allow operation at lower recoveries since certain membranes in the configurations will be operated below the minimum concentrate flow when the recovery is reduced back to 80%. Furthermore, the current configuration and space limitations of the plant on RO Pass 1 will require numerous other modifications to be made to existing structures, electrical and instrumentation work. This solution is expensive, difficult to execute and most importantly will not allow for flexible operation at various recovery rates thereby, eliminating this solution.

The preferred solution is to instal an additional line with a control valve which will divert a portion of the common reject flow back to the RO Pass 1 feed tank. Controlling the flow rate of reject recovery to the feed of RO 1 the effective recovery over the RO 1 can be controlled to any recovery value. With this solution, the recovery to each RO 1 skid will still be controlled to the original design recovery rate between 80% and 84% making sure that the recovery, and maximum and minimum flow of each membrane in the system are within the limits. The additional line will be less expensive than additional vessels and the line can be routed within the current plant configuration without impacting existing equipment and structures. This option allows for a high degree of flexibility as the recovery can be changed at any given time by the plant operator based on changing feed water qualities.

5.2.2 RO Pass 2 optimisation

When evaluating the reference plant data (Figure 1-2) the feed water to RO Pass 2 quality will always be in the low feed concentration range, between 2 to 20 mg/L. The low feed quality also means that the scaling potential on RO Pass 2 is negligible. Therefore, the solution is focused on the layout to remove or reduce the current physical limitations of the system to operate at the highest possible flux and recovery.

The only available option is to find the maximum recovery available with the lowest possible additional vessels and membranes. With the addition of 1 vessel configured as a 3rd stage the recovery over each RO Pass 2 skid can be increased from the current 85% to 94%. With this modification, the 94% recovery of each skid can be reached without exceeding the recovery and flux limitations of the membranes on any of the stages. This solution was found to be the most optimum since the additional vessel can be easily accommodated with enough space already available and only minor pipe routing modifications is required.

5.2.3 Optimisation results

Implementing the proposed solutions for both RO Pass 1 and Pass 2 and operating with Water A the plant's capabilities can potentially be improved as shown in Table 5-1.

Table 5-1: Results from reference plant configuration optimisation, calculated in WAVE™

	Unit	Design values	Optimised values
RO Pass 1			
Effective recovery		80%	96%
Feed flow rate [5]	m^3/h	159	159
Reject flow	m^3/h	31.8	6.3
RO Pass 2			
Effective recovery		85%	94%
Feed flow rate	m^3/h	86	101.7
Reject flow rate	m^3/h	12.9	6.1
Permeate flow rate	m^3/h	73.1	94.7
Filtered water required for RO 2 permeate flow	**m^3/h**	**94.6**	**98.8**
Filtered water to Demineralised recovery		**77.3%**	**95.8%**

The demineralised production (RO pass 2 permeate) output can be increased from 365 m^3/h (73.1 x 5 skids) to 473 m^3/h, a 23% increase in production capacity. In other words, the modifications will allow the plant to produce 107 m^3/h (23%) more demineralised water and only require 21 m^3/h (4%) more raw water compared to the current configuration.

5.2.4 Conclusion on reference plant optimisation

The proposed optimisation changes are not only a production volume increase but also a decrease in effluent production. Increasing the overall plant recovery from 77% to almost 96% will reduce the effluent production by the water plant by 80%. This reduction in effluent water from the water treatment plant can have a major positive impact on the power station's ability to meet its water usage targets set out in the water management plan (Eskom, 2018). Furthermore, the proposed changes are not intrusive and relatively small changes which will allow for ease of implementation with minimum downtime requirements. The benefits of the proposed modifications to RO Pass 1 and Pass 2 are well demonstrated in Table 5-1 therefore, the proposed modifications are recommended for implementation.

[5] The reference plant RO pass 1 is oversized supplying other process as well, therefore the permeate from RO pass 1 is not equal to the feed flow to RO pass 2

CHAPTER 6 CONCLUSION AND RECOMMENDATIONS

6.1 Conclusion

The operational experience of the reference reverse osmosis plant over a wide range of feed water concentrations formed the base of this investigation. Therefore, an experimental single module membrane rig was used to replicate the operational plant in a more controlled environment with a single reference salt, NaCl, at various concentrations and operating conditions. The results are used to construct a predictive model that can determine the main membrane performance parameters across the whole feed concentration range tested. This allowed the evaluation of the membranes on equal footing based on their water and salt permeability constants calculated in the model work. From the results, Toray is the membrane showed the lowest salt permeability and the highest water permeability, therefore it is the preferred membrane under the tested conditions.

The reduced salt rejection at lower feed concentrations is explained, and accounted for in the model, due to the reduction of the Donnan effect at the lower feed concentrations. Additional equations presented by Anisimov & Orlov (2018) were added to the standard solution diffusion model, and the experimental and modelling results confirmed the change in Donnan effect as the reduction in salt rejection for feed concentrations lower than 100 mg/L. Since the Donnan effect is a thermodynamic property related to ions in solutions, the lower salt rejection at low and high feed concentrations with a definite optimum feed concentration, is an intrinsic property of RO membranes. This is important information used in the optimisation of the reference plant.

The different suppliers' modelling software (WAVE™, IMSDesign© and DS2©) results correlated well with the experimental measurements, providing confidence in the software which is used to conduct an optimisation exercise on the reference plant. From the optimisation exercise, two modifications were recommended: one to RO Pass 1 and one to RO Pass 2, to allow flexibility for the plant to operate at the maximum possible recovery for any given feed quality over the possible concentration range. The modifications can potentially increase the plant production by 23% and reduce the wastewater (effluent) by 80%.

6.2 Contribution to science

The results presented provided additional information on the operation of RO brackish water membranes at low feed concentrations to the academic community. The performance characteristics for RO membranes are mostly researched and developed by the suppliers and the information is not available to the academic community, and this knowledge is seen as Intellectual Property (IP) to gain or maintain an advantage over the competition. This is demonstrated by each supplier keeping its membranes' performance within its modelling software and then making limited with only two usable publications (Anisimov & Orlov, 2018; Bartels *et al.*, 2005) publishing results for RO membranes operating at lower than 500 mg/L feed concentrations.

The results from this study confirmed that two additional terms can accurately model the membrane's performance throughout the feed concentrations. Since no other reference studies could be found for the modelling equations presented by Anisimov & Orlov (2018), the results serve as a confirmation of their validity to predict the reduced impact of the Donnan effect at low concentrations.

6.3 Recommendations

Should further testing be done on the experimental setup, it is recommended to include temperature control measures since this proved to complicate the analysis of the results. Although the repeatability of the experiment and the number of data points were adequate, more data would further increase the confidence and accuracy of the model. It is also recommended to modify the rig so that the feed flow rates can be increased to allow the skid to operate at a higher membrane flux. As demonstrated by modelling, the increase in flux and feed pressure will also assist with better salt rejection.

Further studies to determine the effect of pH on the membrane rejection and in particular the lower feed concentration range could add value to the scientific knowledge for RO membranes. The difference in performance of the three membranes was not investigated since the full characterisation of the membranes was not part of the scope. It is therefore recommended that a further study can be performed to examine the difference between the membranes based on the properties of the membrane. The membranes were deliberately fouled by drying the membranes and exposing it to atmospheric conditions (Section 3.4), further studies can be done to test and/or develop a Clean in Place (CIP) protocol to in attempt to reverse the fouling.

Lastly, the modifications to the reference plant detailed in Chapter 5 should be implemented to improve the plant's performance in terms of production capacity, water recovery and ultimately water usage.

BIBLIOGRAPHY

Abdulsalam Ebrahim, M., Karan, S. & Livingston, A.G. 2020. On the influence of salt concentration on the transport properties of reverse osmosis membranes in high pressure and high recovery desalination. *Journal of Membrane Science*, 594:117339. https://www.sciencedirect.com/science/article/pii/S0376738818329557 https://doi.org/10.1016/j.memsci.2019.117339

Alsarayreh, A.A., Al-Obaidi, M.A., Farag, S.K., Patel, R. & Mujtaba, I.M. 2021. Performance evaluation of a medium-scale industrial reverse osmosis brackish water desalination plant with different brands of membranes. A simulation study. *Desalination*, 503:114927. https://www.sciencedirect.com/science/article/pii/S0011916420316052 https://doi.org/10.1016/j.desal.2020.114927

Anisimov, S.I. & Orlov, N.S. 2018. Study of Mass Transfer during Reverse-Osmosis Demineralization of Dilute Solutions of Strong Electrolytes. *Petroleum Chemistry*, 58(13):1107-1112.

ASTM. 2019. Standard Practice for Standardizing Reverse Osmosis Performance Data. West Conshohocken, PA: ASTM International.

Atkins, P. & de Paula, J. 2002. *Atkins' Physical Chemistry*. London: Oxford University Press.

Bartels, C., Franks, R., Rybar, S., Schierach, M. & Wilf, M. 2005. The effect of feed ionic strength on salt passage through reverse osmosis membranes. *Desalination*, 184:185-195.

Byrne, W. 2002. *Reverse Osmosis A Practical guide for industrial users*. Littleton: Tall Oaks Publishing.

Chen, C. & Qin, H. 2019. A Mathematical Modeling of the Reverse Osmosis Concentration Process of a Glucose Solution. *Processes*, 7:271. 10.3390/pr7050271

Ding, M., Szymczyk, A., Goujon, F., Soldera, A. & Ghoufi, A. 2014. Structure and dynamics of water confined in a polyamide reverse-osmosis membrane: A molecular-simulation study. *Journal of Membrane Science*, 458:236-244.

Donnan, F.G. 1995. Theory of membrane equilibria and membrane potentials in the presence of non-dialysing electrolytes. *Journal of Membrane Science*, 100:45-55.

DOWA. 2008. *MOKOLO AND CROCODILE (WEST) WATER AUGMENTATION PROJECT (MCWAP) Feasibility Study*.

DuPont. 2016. *FILMTEC™ Reverse Osmosis Membranes Technical Manual*.

DuPont. 2019. *Tech Fact - Factors Affecting RO Membrane Performance*

DuPont. 2022. *WAVE Water Treatment Design Software*. https://www.dupont.com/water/resources/design-software.html Date of access: 2022-09-26.

Ebrahim, M.A., Karan, S. & Livingston, A.G. 2020. On the influence of salt concentration on the transport properties of reverse osmosis membranes in high pressure and high recovery desalination. *Journal of Membrane Science*, 594,

Eke, J., Yusuf, A., Giwa, A. & Sodiq, A. 2020. The global status of desalination: An assessment of current desalination technologies, plants and capacity. *Desalination*, 495(114633),

EPRI. 2019. *Membrane Treatment Guideline*. Palo Alto, CA.

Eskom. 2018. *Data and information used from Eskom-specific sources with permission* [Dataset].

Eskom. 2021a. *Eskom Sustainability Report 2021*.

Eskom. 2021b. *Eskom Integrated Report 2021*.

Galama, A.H., Post, J.W., Cohen Stuart, M.A. & Biesheuvel, P.M. 2013. Validity of the Boltzmann equation to describe Donnan equilibrium at the membrane–solution interface. *Journal of Membrane Science*, 442:131-139. https://www.sciencedirect.com/science/article/pii/S0376738813003025 https://doi.org/10.1016/j.memsci.2013.04.022

Haidari, A.H., Heijman, S.G.J. & van der Meer, W.G.J. 2018. Optimal design of spacers in reverse osmosis. *Separation and Purification Technology*, 192:441-456.

Hung, L.-Y., Lue, S.J. & You, J.-H. 2011. Mass-transfer modelling of reverse-osmosis performance on 0.5–2% salty water. *Desalination*, 265(1):67-73. https://www.sciencedirect.com/science/article/pii/S001191641000531X https://doi.org/10.1016/j.desal.2010.07.033

Hydranautics. 2022. *IMSDesign Integrated membrane solutions*. https://membranes.com/solutions/software-imsdesign/ Date of access: 2022-11-23.

Hyung, H. & Kim, J.-H. 2006. A mechanistic study on boron rejection by seawater reverse osmosis membranes. *Journal of Membrane Science*, 286(1):269-278. https://www.sciencedirect.com/science/article/pii/S0376738806006569 https://doi.org/10.1016/j.memsci.2006.09.043

Jang, E.-S., Mickols, W., Sajunani, R., Alysha, H., Dilenschneider, T.J., Kamcer, J., ... Freeman, B.D. 2019. Influence of concentration polarization and thermodynamic non-ideality on salt transport in reverse osmosis membranes. *Journal of Membrane Science*, 572:668-675.

Jawor, A. & Hoek, E.M.V. 2009. Effects of feed water temperature on inorganic fouling of brackish water RO membranes. *Desalination*, 235(1):44-57. https://www.sciencedirect.com/science/article/pii/S0011916408005845 https://doi.org/10.1016/j.desal.2008.07.004

Jin, X., Jawor, A., Kim, S. & Hoek, E.M.V. 2009. Effects of feed water temperature on separation performance and organic fouling of brackish water RO membranes. *Desalination*, 239(1):346-359. https://www.sciencedirect.com/science/article/pii/S0011916409000484 https://doi.org/10.1016/j.desal.2008.03.026

Kim, S. & Hoek, E.M.V. 2005. Modelling concentration polarization in reverse osmosis processes. *Desalination*, 186(1):111-128. https://www.sciencedirect.com/science/article/pii/S0011916405006867 https://doi.org/10.1016/j.desal.2005.05.017

Lee, H., Jin, Y. & Hong, S. 2016. Recent transitions in ultrapure water (UPW) technology: Rising role of reverse osmosis (RO). *Desalination*, 399:185-197.

Li, M. 2012. Optimal plant operation of brackish water reverse osmosis (BWRO) desalination. *Desalination*, 293:61-68.

Li, M. 2019. Predictive modelling of a commercial spiral woundseawater reverse osmosis module. *Chemical Engineering Research and Design*, (148):440-450.

Li, M., Bui, T. & Chao, S. 2016. Three-dimensional CFD analysis of hydrodynamics and concentration polarization in an industrial RO feed channel. *Desalination*, 397:194-204.

Maddah, H. & Almugahwi, M. 2017. *Application of The Solution-Diffusion Model to Optimize Water Flux in Reverse Osmosis Desalination Plants*.

Mai, Z., Gui, S., Fu, J., Jiang, C., Ortega, E., Zhao, Y., ... Van der Bruggen, B. 2019. Activity-derived model for water and salt transport in reverse osmosis membranes: A combination of film theory and electrolyte theory. *Desalination*, 469,

Mandel, J. & Lashof, T.W. 1987. The Nature of Repeatability and Reproducibility. *Journal of Quality Technology*, 19(1):29-36. https://doi.org/10.1080/00224065.1987.11979030 10.1080/00224065.1987.11979030

Mickols, W., Mai, Z. & van der Bruggen, B. 2021. Effect of pressure and temperature on solvent transport across nanofiltration and reverse osmosis membranes: An activity-derived transport model. *Desalination*, 501:114905. https://www.sciencedirect.com/science/article/pii/S0011916420315836 https://doi.org/10.1016/j.desal.2020.114905

Okamoto, Y. & Lienhard, J.H. 2019. How RO membrane permeability and other performance factors affect process cost and energy use: A review. *Desalination*, 470:114064. https://www.sciencedirect.com/science/article/pii/S0011916419305752 https://doi.org/10.1016/j.desal.2019.07.004

Richards, L., Schaefer, A., Richards, B.S. & Corry, B. 2012. The Importance of Dehydration in Determining Ion Transport in Narrow Pores. *Small*:1701-1709.

Sengupta, S.S. & Prakash, P. 2010. The Donnan membrane principle can permit many engineered processes and materials to achieve better sustainability. *Environmental Science & Technology*, 44:1161-1166.

Shahid, M.K. & Choi, Y.-G. 2018. The comparative study for scale inhibition on surface of RO membranes in wastewater reclamation: CO2 purging versus three different antiscalants. *Journal of Membrane Science*, 546:61-69. https://www.sciencedirect.com/science/article/pii/S0376738817316228 https://doi.org/10.1016/j.memsci.2017.09.087

Shen, M., Keten, S. & Lueptow, R.M. 2016. Dynamics of water and solute transport in polymeric reverse osmosis membranes via molecular dynamics simulations. *Journal of Membrane Science*, 506:95-108.

Shenvi, S.S., Isloor, A.M. & Ismail, A.F. 2015. A review on RO membrane technology: Developments and challenges. *Desalination*, 2015:10-26.

Srivathsan, G., Sparrow, E.M. & Gorman, J.M. 2014. Reverse Osmosis issues relating to pressure drop, mass transfer, turbulence, and unsteadiness. *Desalination*, 341:83-86.

SWESN. 2021. *Report on Sustainable Water and Energy Solutions Addressing Climate Change*.

Taniguchi, M., Kurihara, M. & Kimura, S. 2001. Behavior of a reverse osmosis plant adopting a brine conversion two-stage process and its computer simulation. *Journal of Membrane Science*, 183(2):249-257. https://www.sciencedirect.com/science/article/pii/S0376738800005974 https://doi.org/10.1016/S0376-7388(00)00597-4

Tansel, B. 2012. Significance of thermodynamic and physical characteristics on permeation of ions during membrane separation: Hydrated radius, hydration free energy and viscous effects. *Separation and Purification Technology*, 86:119-126.

Toray. 2022. *Toray DS - new RO Design software*. https://www.water.toray/knowledge/tool/ds/ Date of access: 2022-11-23.

Wagner, H. 2012. Influence of temperature on electrical conductivity of diluted aqueous solutions. 92:82-89.

Wang, L., Dlamini, D.S., Mishra, A.K., Pndergaste, M.T.M., Wong, M.C.Y., Mamba, B.B., ... Hoek, E.M.V. 2014. A critical review of transport through osmotic membranes. *Journal of Membrane Science*, 454:516-537.

Zhangxin Wang, A.D., Yuhao Du, Menachem Elimelech. 2020. Minimal and zero liquid discharge with reverse osmosis using low-salt-rejection membranes. *Water Research*, 170(115317), https://doi.org/10.1016/j.watres.2019.115317

APPENDIX A PLANT CONFIGURATION

The reference plant consists of a two-pass RO system. RO Pass 1 consists of 6 skids, each skid delivers 20% of the design permeate flow rate therefore, 5 skids are required to produce the required permeate flow rate. All 6 skids are identical, with 8" FILMTEC™ BW30XFR-400/34i membranes installed on all stages. Each membrane vessel holds 6 individual membranes. Each skid has 3 stages, 12 vessels on stage 1, 6 vessels on stage 2 and 4 vessels on stage 3. Figure A-1 provides a process diagram for the plant configuration.

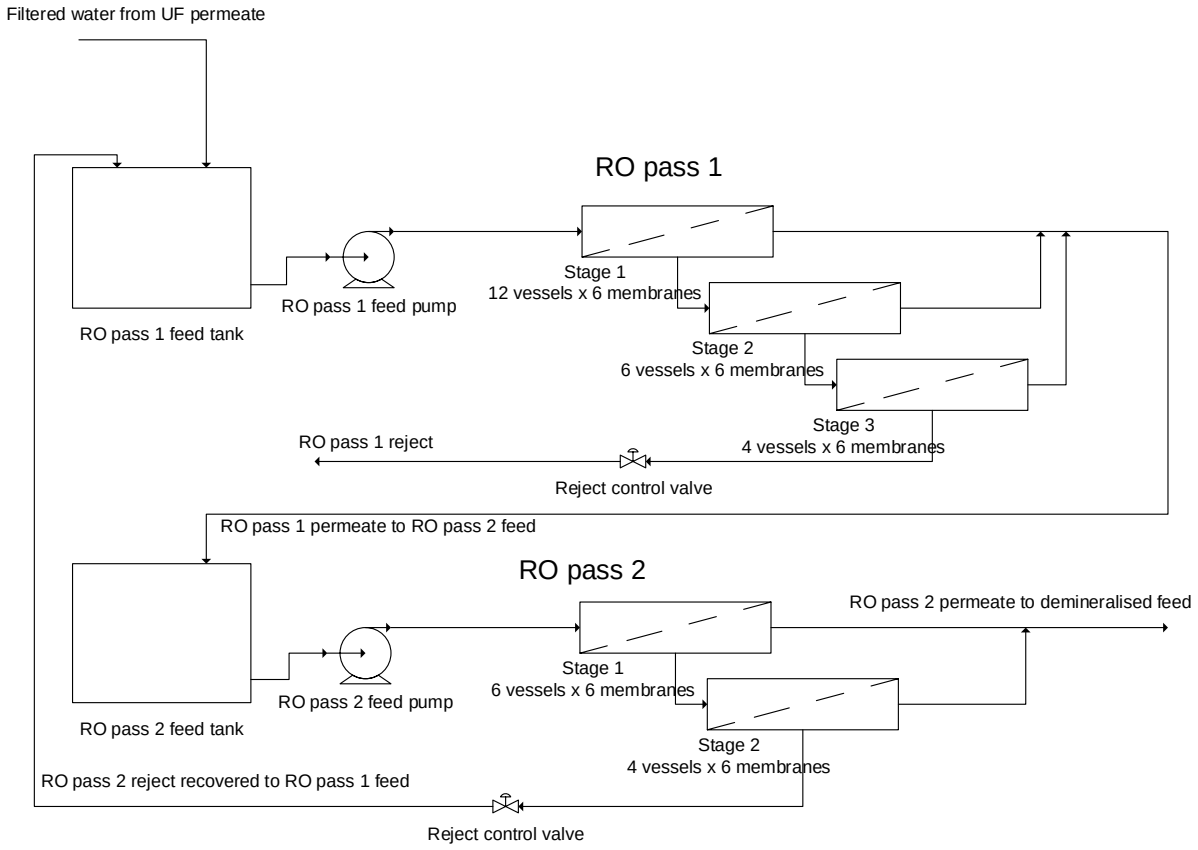

Figure A-1: Configuration of one RO pass 1 and pass 2 skids for the reference plant

The overall design recovery for RO 1 is 80%, which is achieved by controlling the reject (retentate) flow rate. Design simulations performed by ROSA (OEM simulation software) in 2016 provided the projected rejection performance for the water qualities and design conditions for the reference plant is shown in Table A-1. The flow factor is used to simulate future possible fouling, therefore, catering for the increase in flow resistance of the membranes in the design. The projected results from the ROSA simulations predicted high rejection rates for all simulated cases, with 97.2% being the worst / lowest rejection rate that was predicted.

The limitation on RO Pass 1 is the flow limit on the first stage, therefore if the recovery or permeate production wants to be increased additional vessels and membranes will be required to be added to the first stage.

Table A-1: ROSA simulation results for RO 1 on average rejection rates at the temperature

Feed water	Feed Conductivity (µS.cm^{-1})	Average Rejection
Water A / Plant A / Flow Factor 0.7 / 15 ^{0}C	173	98.4%
Water A / Plant A / Flow Factor 1 / 15 ^{0}C	172	98.4%
Water A / Plant A / Flow Factor 0.7 / 20 ^{0}C	172	97.9%
Water A / Plant A / Flow Factor 1 / 20 ^{0}C	172	97.9%

RO Pass 2 also consists of 6 skids. Each skid delivers 20% of the design permeate flow rate; therefore 5 skids are required to produce the required permeate flow rate. All 6 skids are identical, with 8" FILMTEC™ BW30XFR-400/34i membranes installed on both stages. Each membrane vessel holds 6 individual membranes. Each skid has 2 stages, 6 vessels on stage 1 and 4 vessels on stage 2.

The 2nd pass produces the demineralised make-up flow rate to the polishing plant before the final demineralised water is sent to the different users of the power plant. The overall design recovery for RO pass 2 is 85%, which is achieved by controlling the reject flow rate of each skid. The reject from RO pass 2 has a lower TDS than that of the feed to RO Pass 1 therefore, the reject is fully recycled to this feed stream to increase the overall water recovery from the plant.

Table A-2 shows the ROSA simulation results for a few design cases for the reference plant. The results show some reduction in the rejection rates as the feed water quality decreases, with the lowest rejection rate predicted being 83.6% at a feed conductivity of 1.9 µS/cm.

Table A-2: ROSA simulation results for RO Pass 2 on average rejection rates at the temperature

Feed water	Feed Conductivity ($\mu S.cm^{-1}$)	Average Rejection
Water A / Plant A / Flow Factor 0.7 / 15 ^{0}C	23.2	94.9%
Water A / Plant A / Flow Factor 1 / 15 ^{0}C	23.2	94.9%
Water A / Plant A / Flow Factor 0.7 / 20 ^{0}C	23.2	93.6%
Water A / Plant A / Flow Factor 1 / 20 ^{0}C	23.2	93.5%
Water A / Plant B / Flow Factor 0.85 / 21 ^{0}C	1.90	83.6%
Water A / Plant B / Flow Factor 0.85 / 25 ^{0}C	11.4	91.8%

APPENDIX B NORMALISATION OF PLANT OPERATIONAL DATA

Operational conditions can vary significantly in terms of feed conductivity, water temperatures, flow rates etc. To compare membrane and plant performance over varying operational conditions a normalised salt passage and feed flow needs to be calculated. The normalisation calculations are done according to international standards (ASTM, 2019) which is the industry-recognised method for normalisation.

Equation B-1 and B-2 is extracts from ASTM D4516-19 for the normalisation of permeate flow and rejection (inverse of salt passage) which applies to this study.

The standardisation of the permeate flow is given by Equation B-1.

$$Q_{ps} = \frac{\left[P_{fs} - \frac{\Delta P_{fbs}}{2} - P_{ps} - \pi_{fbs} + \pi_{ps}\right](TCF_s)}{\left[P_{fa} - \frac{\Delta P_{fba}}{2} - P_{pa} - \pi_{fba} + \pi_{pa}\right](TCF_a)}\left(Q_{pa}\right) \qquad \text{B-1}$$

Q_{ps} = permeate flow at standard conditions

P_{fs} = feed pressure at standard conditions, kPa

$\frac{\Delta P_{fbs}}{2}$ = one half devise pressure drop at standard conditions, kPa

P_{ps} = permeate pressure at standard conditions, kPa

π_{fbs} = feed-brine osmotic pressure at standard conditions, kPa

π_{ps} = permeate osmotic pressure at standard conditions, kPa

TCF_s = Temperature correction factor at standard conditions

Q_{pa} = permeate flow at actual conditions

P_{fa} = feed pressure at actual conditions, kPa

$\frac{\Delta P_{fba}}{2}$ = one half devise pressure drop at actual conditions, kPa

P_{pa} = permeate pressure at actual conditions, kPa

π_{fba} = feed-brine osmotic pressure at actual conditions, kPa

π_{pa} = permeate osmotic pressure at actual conditions, kPa

TCF_a = Temperature correction factor at actual conditions

The standardisation equation for salt passage is given by Equation B-2

$$\%SP_s = \left[\frac{EPF_a}{EPF_s}\right] \times \left[\frac{STCF_a}{STCF_s}\right] \times \left[\frac{C_{fbs}}{C_{fba}}\right] \times \left[\frac{C_{fa}}{C_{fs}}\right] \times \%SP_a \qquad \text{B-2}$$

$\%SP$ = percentage salt passage normalised to standard conditions

$\%SP_a$ = percent salt passage at actual conditions

EPF_s = average element permeate flow at standard conditions

EPF_a = average element permeate flow at actual conditions

$STCF_s$ = salt transport temperature correction factor at standard conditions

$STCF_a$ = salt transport temperature correction factor at actual conditions

C_{fbs} = feed-brine concentration at standard conditions, mg/L

C_{fba} = feed brine concentration at actual conditions, mg/L

C_{fs} = feed concentration at standard conditions

C_{fa} = feed concentration at actual conditions

APPENDIX C SAMPLE CALCULATION AND REPEATABILITY

C.1 Sample calculation

A sample calculation is done from one sample collected during Data set 2 for Toray membranes on 2021/11/03 at 17:13. The sample calculation is done as described in Section 3.2.2.

Date	Time	Feed Pressure	Permeate Pressure	Permeate Mass	Permeate Time	Analyser flow	Reject Time	Reject Mass	Feed	Permeate	Temp
YYYY-MM-DD	HH:MM	kPa	kPa	g	s	L/h	s	kg	µS/cm	µS/cm	°C
2021/11/03	17:13	482.9	19.529	1400	31.07	23.3	30	6.99	177	0.796	31.1

$$Permeate\ flow = Analyser\ flow + \left(\frac{Permeate\ Mass}{1000} / Permeate\ Time\right) * 60 * 60 = 185.5\ L/h$$

$$Reject\ flow = \ (Reject\ Mass / Reject\ Time) * 60 * 60 = 838.8\ L/h$$

$$Feed\ flow = Permeat\ flow + Reject\ flow = 1024\ L/h$$

For both flow measurements, the density of the liquid was assumed to be 1000 kg/m^3 for the conversion from kg to L.

The scale error is 0.01 kg and assuming a maximum error of 0.5s in the stopwatch reading the permeate flow error is calculated at 2.1% and the reject flow rate at 1.8%.

Conversion of feed and permeate Conductivity to NaCl concentration:

$$C_F = \ Feed\ Conductivity * 0.462 = \frac{82\frac{mg}{L}}{1000} / \frac{58.35g}{mol} = 1.40x10^{-3}\frac{mol}{L}$$

$$C_p = Permeate\ Conductivity * 0.462 = \frac{0.37\frac{mg}{L}}{1000} / \frac{58.35g}{mol} = 6.32x10^{-6}\frac{mol}{L}$$

Observed rejection

$$R_o = 1 - \frac{C_p}{C_f} = 1 - \frac{0.37\frac{mg}{L}}{82\frac{mg}{L}} * 100 = 99.6\%$$

Calculation of experimental water flux:

$$J_w = \frac{Permeate\ flow}{Membrane\ Area} = \frac{185.5}{8} = 23.2\frac{L}{m^2.h} * \frac{1}{1000 * 60 * 60} = 6.4415x10^{-6}\frac{m}{s}$$

Experimental calculated solute flux:

$$J_s = C_p * J_w = 6.32x10^{-6}\frac{mol}{L} * \ 23.2\frac{L}{m^2.h} = 1.46x10^{-4}\frac{mol}{m^2.h}$$

For the Re, Sc and Sh numbers the following parameters are required:

From Equation 2-12 and Table 3-1 the velocity is calculated as follows:

$$u = \frac{Q}{n_c H \epsilon L} = \frac{Permeate\ flow}{1000 * 3600}\frac{m^3}{s} * \frac{1}{23 * 8.636x10^{-4}m * 0.905m * 0.94} = 0.00305\frac{m}{s}$$

From Equation 2-15 the salt diffusion coefficient is calculated:

$$D_s = 6.725 \cdot 10^{-6} \cdot exp\left(0.1546 \cdot 10^{-3} \cdot \frac{82mg}{L} - \frac{2513}{273.15 + 31.1^0C}\right) = 1.7401x10^{-9}\frac{m^2}{s}$$

Equation 2-11:

$$Re = \frac{ud_H\rho}{v} = \frac{0.00305\frac{m}{s} * 0.00157m * 997.047\frac{kg}{m^3}}{0.0089\frac{kg}{m.s}} = 5.37$$

Equation 2-14:

$$Sc = \frac{v}{\rho D_s} = \frac{0.0089\frac{kg}{m.s}}{997.047\frac{kg}{m^3} * 1.7401x10^{-9}\frac{m^2}{s}} = 513.03$$

C.2 Repeatability of measurement

For each sampled operating point in terms of recovery (determined by permeate flow) and feed concentrations (feed conductivity) 3 measurements of the permeate and reject flow and feed and reject conductivity were done. The repeatability of the measurements is assessed by calculating the standard deviation (s). In Table C-1 the standard deviation is calculated for the measurement of each sampled operating point. The average standard deviation is then converted to a repeatability (r) measurement given by Equation C-1 with k equal to 1.96 and s the standard deviation (Mandel & Lashof, 1987).

$$r = k\sqrt{2}s \qquad \text{C-1}$$

The repeatability value (r) for a 95% confidence level the feed flow is 3.2 L/h, reject flow is 11.2 L/h, feed conductivity is 6.4 µS/cm and the permeate conductivity 0.1 µS/cm. The permeate conductivity is very low due to the very small variance in between measurements (s = 0.03).

Table C-1: Sample repeatability calculation for Hydranautics data set

Date	Time	Permeate Flow	Permeate Flow St Dev	Reject Flow	Reject Flow St Dev	Feed Conductivity	Feed Conductivity St Dev	Permeate Conductivity	Permeate Conductivity St Dev
YYYY-MM-DD	HH:MM	L/h		L/h		µS/cm		µS/cm	
2021/10/20	14:15	194.2		1022.4		29.4		0.749	
2021/10/20	14:19	195.1	1.48	1023.6	5.92	29.5	0.06	0.747	0.00
2021/10/20	14:23	192.2		1012.8		29.5		0.750	
2021/10/20	14:27	157.8		922.8		29.8		0.781	
2021/10/20	14:31	161.0	1.74	924.0	1.83	29.8	0.00	0.779	0.00
2021/10/20	14:35	160.7		926.4		29.8		0.780	
2021/10/20	14:51	160.3		925.2		96.3		1.15	
2021/10/20	14:55	161.1	0.46	916.8	4.21	96.2	0.21	1.14	0.01
2021/10/20	14:58	161.2		920.6		95.9		1.15	
2021/10/20	15:01	193.4		1008.0		96.2		1.05	
2021/10/20	15:05	196.7	2.46	1006.8	2.50	96.3	0.21	1.06	0.01
2021/10/20	15:08	198.2		1011.6		95.9		1.06	
2021/10/20	15:25	194.5		1009.2		207		1.59	
2021/10/20	15:29	197.9	2.33	1005.6	1.83	207	0.58	1.60	0.01
2021/10/20	15:32	199.0		1008.0		208		1.58	
2021/10/20	15:35	160.3		919.2		207		1.75	
2021/10/20	15:38	160.0	0.32	910.8	4.21	207	0.00	1.76	0.01
2021/10/20	15:41	160.6		915.6		207		1.76	
2021/10/20	15:58	154.1		924.0		772		5.16	
2021/10/20	16:01	154.5	0.30	914.4	6.82	768	2.65	5.10	0.03
2021/10/20	16:03	154.7		927.6		767		5.12	
2021/10/20	16:08	187.6		1015.2		773		4.41	
2021/10/20	16:11	187.6	0.91	1016.4	0.69	766	3.61	4.37	0.05
2021/10/20	16:14	189.1		1016.4		768		4.31	
2021/10/20	16:30	175.7		1032.0		1950		11.1	
2021/10/20	16:34	177.1	0.74	1029.6	1.39	1960	10.00	11.0	0.10
2021/10/20	16:37	176.0		1029.6		1940		10.9	
2021/10/20	16:40	143.9		937.2		1950		12.6	
2021/10/20	16:43	144.0	0.95	943.2	11.15	1950	5.77	12.5	0.10
2021/10/20	16:45	142.3		958.8		1960		12.4	
Average St Deviation			**1.2**		**4.1**		**2.3**		**0.03**
Repeatability (k.√2.s)			**3.2**		**11.2**		**6.4**		**0.1**

APPENDIX D OPTIMISATION SIMULATION RESULTS

The antiscalant supplier's calculations for the recovery limit for water source A as it was determined during the optimisation of the reference plant in 2015. The suppliers calculated the maximum possible recovery based on the water quality scaling potential as the reject stream is concentrated. The calculation is done with antiscalant dosing at the recommended dosage rate. This limit was used in the optimisation exercise to achieve the highest possible RO 1 recovery.

Flodose by Marleen Theunissen **Page: 1**

Program Version: 4.0 BWA File version: 3.05
Project: Eskom Print Date: 12-Jun-15
Project File: Analysis File:
Engineer: Marleen Theunissen Client: Marleen Theunissen

User Selection:	**FLOCON 260**	
Recommended Dose Rates:	1.0 mg/l - Feed,	33.3 mg/l - Conc.
Est. FLOCON 260 usage (100%):	3.84 kgs/day	1.4026 mt/yr
Est. Acid Dose (100%):	Sulphuric Acid	8.0 ppm - Feed
pH Control Method:	Flodose recommended a Feed pH of:	6.79
Est. Acid usage (100%):	30.66 kgs/day	11.1983 mt/yr

System Information	**Flow Units: m3/hr**		
Feedwater Type:	Surface/Lake Water		
Feedwater Flow:	160.0	Concentrate Flow:	4.8
Permeate Flow:	155.2	Recycle Flow:	0.0
System Recovery:	97.00%	RO Recovery:	97.00%
RO Membrane Type:	Thin Film High Rejection	Membrane Rejection:	99.22%

mg/l, 25.0 C	**Raw Feed**	**Treated Feed**	**Average Feed**	**Product**	**Concentrate**
Ca++	8.18	8.18	73.35	0.12	263.94
Mg++	2.36	2.36	21.15	0.04	76.08
Na+	4.42	4.42	38.25	0.21	135.91
K+	1.67	1.67	14.40	0.09	51.09
NH4+	0.05	0.05	0.40	0.01	1.36
Ba++	0.02	0.02	0.18	0.00	0.65
Sr++	0.02	0.02	0.18	0.00	0.65
Fe2+/3+	0.00	0.00	0.00	0.00	0.00
Al+++	0.00	0.00	0.00	0.00	0.00
HCO3-	37.16	27.96	238.97	1.75	836.70
Cl-	5.43	5.43	46.99	0.29	166.99
SO4--	4.17	11.99	107.40	0.21	386.28
F-	0.29	0.29	2.57	0.01	9.23
NO3-	0.09	0.09	0.74	0.01	2.57
PO4---	0.00	0.00	0.00	0.00	0.00
SiO2	0.12	0.12	1.07	0.01	3.81
CO3--	0.36	0.01	0.78	0.00	12.26
CO2	0.30	7.21	7.17	7.20	7.10
TDS	64.34	62.61	553.29	2.73	1,947.51
Ionic Strength	0.00	0.00	0.01	0.00	0.04
pH	8.29	6.79	7.69	5.71	8.22

Saturation Index (SI)	**Raw Feed**	**Treated Feed**	**Con-centrate**	**% Max SI FLOCON 260**
LSI	-0.541	-2.176	1.937	74.49%
SDSI	-0.637	-2.271	1.973	78.92%
CaSO4	0.000	0.000	0.166	4.15%
BaSO4	0.043	0.123	39.596	33.00%
SrSO4	0.000	0.000	0.025	0.21%
Caf2	0.000	0.000	0.195	0.16%
SiO2	0.001	0.001	0.023	0.77%
Iron	0.000	0.000	0.000	0.00%
Aluminum	0.000	0.000	0.000	0.00%

No Warnings Noted provided FLOCON 260 dosing is maintained.

Program Version: 4.0 BWA File version: 3.05
Project: Eskom Print Date: 12-Jun-15
Project File: Analysis File:
Engineer: Marleen Theunissen Client: Marleen Theunissen

FLOCON 260
Day Tank and Dosing Pump Design and Information

Note: The dose and tank input data can be changed by the user.
Therefore, it may not match the FLOCON 260.

Feed Dose:	1.0	ppm
Concentrate Dose:	33.3	ppm
System Feed Flow:	160.0	m3/hr
Mass Flow of FLOCON 260:	3.84	kg/day
% Active FLOCON 260:	100.00%	
Dose Pump Rate:	1.58	Liter/hr
Day Tank Volume:	100.0	liter
Day Tank Volume:	2.64	Days of storage
% Active in Day Tank	10.00%	
Volume Water to Fill Day Tank:	91.2	liter
Mass Chemical to Fill Day Tank:	10.1	kg
Volume Chemical to Fill Day Tank:	8.78	liter

Below are the results from the simulations that were done on WAVE™ modelling software. The results presented here is only the preferred optimised solution extracted from the modelling software. The different flow rates and recycle streams with all the detailed predicted operating parameters are shown by the software in the results. There is only one design warning which is flagged by the software, the limit is only slightly exceeded by 0.01 m^3/h (1%) and therefore not a concern.

WATER APPLICATION VALUE ENGINE

WATER SOLUTIONS

WAVE Program Version: 1.82.824

Calculation Engine Version: 01.12.20.03

Database Version: 39

Project Name:	Masters Concentrate up
Case Name:	Case 6: Maximum RO 1 Recovery and RO 2 3rd Stage
Customer:	
Prepared by:	Philip Du Toit
Company:	Eskom
Country:	
Date Created:	August 01, 2022
Project Notes:	Masters simulation for increasing concentration of feedwater to optimised point.
Case #:	6 of: 6
Case Notes:	Case 6
Keywords:	

RO Detailed Report

RO System Flow Diagram

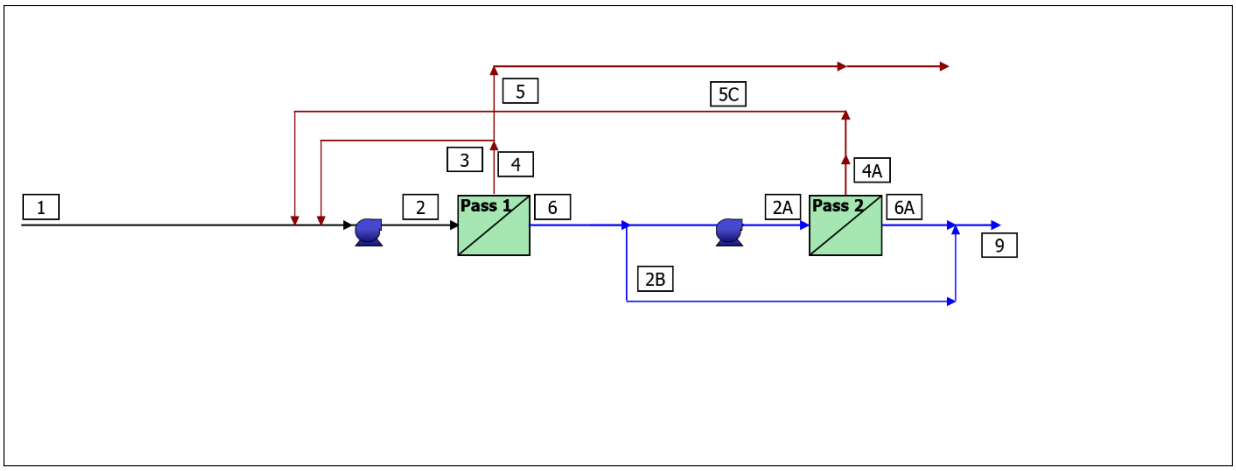

#	Description	Flow (m³/h)	TDS (mg/L)	Pressure (bar)	#	Description	Flow (m³/h)	TDS (mg/L)	Pressure (bar)
1	Raw Feed to RO System	128.0	108.7	0.0	2A	Net Feed to Pass 2	100.7	12.80	12.5
2	Net Feed to Pass 1	159.6	429.7	9.4	2B	Bypass from Pass 2 Feed to Pass 2 Permeate	27.0	12.80	0.0
3	Concentrate Recycle from Pass 1 to Pass 1	25.6	2,095	6.0	4A	Total Concentrate from Pass 2	6.05	165.2	9.2
4	Total Concentrate from Pass 1	31.9	2,095	6.0	5C	Concentrate Recycle from Pass 2 to Pass 1	6.05	165.2	9.2
5	Net Concentrate from RO System	6.33	2,095	6.0	6A	Total Permeate from Pass 2	94.7	3.05	1.0
6	Total Permeate from Pass 1	127.7	12.80	1.0					
9	Net Product from RO System	121.7	5.21						

RO System Overview

Total # of Trains	1	Online =	1	Standby =	0	RO Recovery	95.1 %
System Flow Rate	(m³/h)	Net Feed =	128.0	Net Product =	121.7		

Pass		Pass 1	Pass 2**
Stream Name		Water Source A	-
Water Type		Surface Water (SDI < 5)	RO Permeate SDI < 1
Number of Elements		132	66
Total Active Area	(m^2)	4905	2453
Feed Flow per Pass	(m^3/h)	159.6	100.7
Feed TDS[a]	(mg/L)	429.7	12.80
Feed Pressure	(bar)	9.4	12.5
Flow Factor Per Stage		1.00, 1.00, 1.00	1.00, 1.00, 1.00
Permeate Flow per Pass	(m^3/h)	127.7	94.7
Pass Average flux	(LMH)	26.0	38.6
Permeate TDS[a]	(mg/L)	12.80	3.05
Pass Recovery		80.0 %	94.0 %
Average NDP	(bar)	6.4	9.8
Specific Energy	(kWh/m^3)	0.41	0.46
Temperature	(°C)	25.0	25.0
pH		8.8	8.6
Chemical Dose		-	-
RO System Recovery		95.1 %	
Net RO System Recovery		95.1%	
Specific Energy	(kWh/m^3)	0.79	

Footnotes:

[a]Total Dissolved Solids includes ions, SiO_2 and B. It does not include NH_3 and CO_2

** Design includes Bypass. Please refer to the RO System Diagram.

RO Flow Table (Stage Level) - Pass 1

Stage	Elements	#PV	#Els per PV	Feed				Concentrate			Permeate			
				Feed Flow (m^3/h)	Recirc Flow (m^3/h)	Feed Press (bar)	Boost Press (bar)	Conc Flow (m^3/h)	Conc Press (bar)	Press Drop (bar)	Perm Flow (m^3/h)	Avg Flux (LMH)	Perm Press (bar)	Perm TDS (mg/L)
1	BW30XFR-400/34i	12	6	159.6	31.6	9.1	0.0	81.3	8.2	0.9	78.3	29.3	1.0	8.68
2	BW30XFR-400/34i	6	6	81.3	0.0	8.0	0.0	48.8	7.1	1.0	32.5	24.3	1.0	15.37
3	BW30XFR-400/34i	4	6	48.8	0.0	6.9	0.0	31.9	6.0	0.9	16.9	18.9	1.0	26.89

RO Solute Concentrations - Pass 1

Concentrations (mg/L as ion)										
		Adjusted Feed		Concentrate			Permeate			
	Raw Feed	Initial	After Recycle	Stage1	Stage2	Stage3	Stage1	Stage2	Stage3	Total to Pass 2
NH_4^+	0.75	0.75	1.67	2.64	3.77	5.09	0.68	0.94	1.26	0.82
K^+	1.72	1.72	6.11	11.44	18.39	27.18	0.57	1.01	1.78	0.84
Na^+	7.96	7.96	31.07	59.84	98.23	148.1	1.20	2.15	3.88	1.80
Mg^{+2}	5.48	5.48	22.17	43.49	72.39	110.6	0.03	0.06	0.11	0.05
Ca^{+2}	8.22	8.22	33.25	65.23	108.6	165.9	0.06	0.11	0.19	0.09
Sr^{+2}	0.12	0.12	0.49	0.95	1.59	2.42	0.00	0.00	0.00	0.00
Ba^{+2}	0.03	0.03	0.12	0.24	0.40	0.61	0.00	0.00	0.00	0.00
CO_3^{-2}	1.97	1.98	8.55	17.51	30.33	48.12	0.13	0.17	0.20	0.16
HCO_3^-	48.03	48.03	187.5	362.2	595.8	900.3	5.17	9.20	16.06	7.63
NO_3^-	0.00	0.00	0.00	0.00	0.00	0.00	0.00	0.00	0.00	0.00
F^-	0.20	0.20	0.81	1.59	2.64	4.03	0.00	0.00	0.01	0.00
Cl^-	12.00	12.00	48.50	95.02	158.0	241.2	0.20	0.37	0.67	0.30
Br^{-1}	0.00	0.00	0.00	0.00	0.00	0.00	0.00	0.00	0.00	0.00
SO_4^{-2}	2.20	2.20	8.90	17.46	29.06	44.41	0.01	0.02	0.04	0.02
PO_4^{-3}	0.00	0.00	0.00	0.00	0.00	0.00	0.00	0.00	0.00	0.00
SiO_2	19.00	19.00	76.77	150.1	249.1	379.5	0.63	1.33	2.64	1.07
Boron	0.05	0.05	0.11	0.18	0.25	0.33	0.04	0.06	0.10	0.05
CO_2	0.11	0.11	0.46	0.92	1.57	2.46	0.01	0.04	0.11	0.03
TDS[a]	108.7	108.7	429.7	834.8	1,380	2,095	8.68	15.37	26.89	12.80
Cond. µS/cm	137	137	518	977	1,570	2,318	12	19	31	16
pH	8.8	8.8	8.7	8.7	8.7	8.6	8.7	8.6	8.4	8.6

Footnotes:

[a]Total Dissolved Solids includes ions, SiO_2 and B. It does not include NH_3 and CO_2

RO Design Warnings

Design Warning	Limit	Value	Pass	Stage	Element	Product
Permeate Flow Rate > Maximum Limit (m^3/h)	1.14	1.15	1	1	1	BW30XFR-400/34i

Special Comments

None

RO Flow Table (Element Level) - Pass 1

Stage	Element	Element Name	Recovery (%)	Feed Flow (m^3/h)	Feed Press (bar)	Feed TDS (mg/L)	Conc Flow (m^3/h)	Perm Flow (m^3/h)	Perm Flux (LMH)	Perm TDS (mg/L)
1	1	BW30XFR-400/34i	8.6	13.3	9.1	429.7	12.2	1.15	30.8	6.66
1	2	BW30XFR-400/34i	9.2	12.2	8.9	469.5	11.0	1.12	30.1	7.30
1	3	BW30XFR-400/34i	9.9	11.0	8.7	516.3	9.94	1.09	29.4	8.06

1	4	BW30XFR-400/34i	10.8	9.94	8.6	572.1	8.87	1.07	28.9	8.96
1	5	BW30XFR-400/34i	11.9	8.87	8.5	640.1	7.82	1.06	28.4	10.04
1	6	BW30XFR-400/34i	13.3	7.82	8.3	725.2	6.77	1.04	28.0	11.39
2	1	BW30XFR-400/34i	7.2	13.6	8.0	834.8	12.6	0.97	26.2	12.21
2	2	BW30XFR-400/34i	7.5	12.6	7.8	898.4	11.6	0.94	25.3	13.31
2	3	BW30XFR-400/34i	7.8	11.6	7.7	969.9	10.7	0.91	24.5	14.55
2	4	BW30XFR-400/34i	8.3	10.7	7.5	1,051	9.84	0.89	23.8	15.94
2	5	BW30XFR-400/34i	8.8	9.84	7.3	1,144	8.98	0.86	23.2	17.53
2	6	BW30XFR-400/34i	9.4	8.98	7.2	1,252	8.13	0.84	22.6	19.39
3	1	BW30XFR-400/34i	6.4	12.2	6.9	1,380	11.4	0.78	20.9	21.35
3	2	BW30XFR-400/34i	6.5	11.4	6.7	1,472	10.7	0.74	20.0	23.33
3	3	BW30XFR-400/34i	6.7	10.7	6.5	1,573	9.97	0.71	19.2	25.54
3	4	BW30XFR-400/34i	6.9	9.97	6.4	1,684	9.28	0.69	18.5	28.01
3	5	BW30XFR-400/34i	7.1	9.28	6.2	1,806	8.62	0.66	17.8	30.80
3	6	BW30XFR-400/34i	7.4	8.62	6.1	1,942	7.98	0.64	17.2	33.97

RO Flow Table (Stage Level) - Pass 2

				Feed				Concentrate			Permeate			
Stage	Element	#PV	#Els per PV	Feed Flow	Recirc Flow	Feed Press	Boost Press	Conc Flow	Conc Press	Press Drop	Perm Flow	Avg Flux	Perm Press	Perm TDS
			PV	(m^3/h)	(m^3/h)	(bar)	(bar)	(m^3/h)	(bar)	(bar)	(m^3/h)	(LMH)	(bar)	(mg/L)
1	BW30XFR-400/34i	6	6	100.7	0.00	12.2	0.0	46.5	11.0	1.1	54.2	40.5	1.0	1.77
2	BW30XFR-400/34i	4	6	46.5	0.00	10.8	0.0	13.5	10.2	0.6	33.0	36.9	1.0	4.04
3	BW30XFR-400/34i	1	6	13.5	0.00	10.0	0.0	6.05	9.2	0.9	7.49	33.6	1.0	8.02

Solute Concentrations - Pass 2

Concentrations (mg/L as ion)									
	Feed	Concentrate			Permeate				
		Stage1	Stage2	Stage3	Stage1	Stage2	Stage3	Total	Blend
NH_4^+	0.82	1.43	3.56	6.78	0.30	0.55	0.95	0.44	0.52
K^+	0.84	1.64	4.77	9.82	0.16	0.36	0.69	0.27	0.40
Na^+	1.80	3.67	11.46	24.49	0.19	0.47	0.93	0.35	0.67
Mg^{+2}	0.05	0.11	0.38	0.85	0.00	0.00	0.00	0.00	0.01
Ca^{+2}	0.09	0.19	0.65	1.46	0.00	0.00	0.00	0.00	0.02
Sr^{+2}	0.00	0.00	0.01	0.02	0.00	0.00	0.00	0.00	0.00

Ba^{+2}	0.00	0.00	0.00	0.00	0.00	0.00	0.00	0.00	0.00
CO_3^{-2}	0.16	0.28	0.63	1.18	0.03	0.08	0.14	0.06	0.08
HCO_3^-	7.63	15.36	46.59	97.66	1.03	2.54	5.25	1.89	3.16
NO_3^-	0.00	0.00	0.00	0.00	0.00	0.00	0.00	0.00	0.00
F^-	0.00	0.01	0.02	0.05	0.00	0.00	0.00	0.00	0.00
Cl^-	0.30	0.65	2.20	4.87	0.01	0.02	0.04	0.01	0.08
Br^{-1}	0.00	0.00	0.00	0.00	0.00	0.00	0.00	0.00	0.00
SO_4^{-2}	0.02	0.04	0.14	0.32	0.00	0.00	0.00	0.00	0.00
PO_4^{-3}	0.00	0.00	0.00	0.00	0.00	0.00	0.00	0.00	0.00
SiO_2	1.07	2.32	7.90	17.61	0.01	0.02	0.06	0.02	0.25
Boron	0.05	0.09	0.22	0.38	0.02	0.04	0.09	0.03	0.03
CO_2	0.03	0.08	0.32	0.79	0.00	0.01	0.01	0.01	0.01
TDS[a]	12.80	25.69	78.33	165.2	1.77	4.04	8.02	3.05	5.21
Cond. µS/cm	16	31	89	184	4	7	12	5	8
pH	8.6	8.5	8.4	8.3	8.8	8.8	8.7	8.8	8.7

Footnotes:

[a]Total Dissolved Solids includes ions, SiO_2 and B. It does not include NH_3 and CO_2

RO Flow Table (Element Level) - Pass 2

Stage	Element	Element Name	Recovery (%)	Feed Flow (m^3/h)	Feed Press (bar)	Feed TDS (mg/L)	Conc Flow (m^3/h)	Perm Flow (m^3/h)	Perm Flux (LMH)	Perm TDS (mg/L)
1	1	BW30XFR-400/34i	9.3	16.8	12.2	12.80	15.2	1.56	41.9	1.33
1	2	BW30XFR-400/34i	10.0	15.2	11.9	13.98	13.7	1.53	41.1	1.46
1	3	BW30XFR-400/34i	11.0	13.7	11.7	15.37	12.2	1.50	40.5	1.62
1	4	BW30XFR-400/34i	12.2	12.2	11.5	17.07	10.7	1.49	40.1	1.81
1	5	BW30XFR-400/34i	13.8	10.7	11.3	19.20	9.22	1.48	39.8	2.05
1	6	BW30XFR-400/34i	16.0	9.22	11.2	21.95	7.74	1.48	39.8	2.37
2	1	BW30XFR-400/34i	12.0	11.6	10.8	25.69	10.2	1.40	37.6	2.64
2	2	BW30XFR-400/34i	13.5	10.2	10.7	28.84	8.84	1.38	37.1	2.99
2	3	BW30XFR-400/34i	15.5	8.84	10.5	32.88	7.47	1.37	36.8	3.43
2	4	BW30XFR-400/34i	18.2	7.47	10.4	38.27	6.11	1.36	36.6	4.03
2	5	BW30XFR-400/34i	22.3	6.11	10.3	45.89	4.75	1.36	36.6	4.90
2	6	BW30XFR-400/34i	28.8	4.75	10.3	57.63	3.38	1.37	36.8	6.30
3	1	BW30XFR-400/34i	9.6	13.5	10.0	78.33	12.2	1.29	34.7	6.26
3	2	BW30XFR-400/34i	10.4	12.2	9.8	85.92	11.0	1.27	34.1	6.83
3	3	BW30XFR-400/34i	11.4	11.0	9.7	95.04	9.73	1.25	33.6	7.48
3	4	BW30XFR-400/34i	12.7	9.73	9.5	106.3	8.49	1.23	33.2	8.24
3	5	BW30XFR-400/34i	14.4	8.49	9.4	120.5	7.27	1.22	33.0	9.15
3	6	BW30XFR-400/34i	16.8	7.27	9.3	139.2	6.05	1.22	32.9	10.30

RO Solubility Warnings

Warning	Pass No
Langelier Saturation Index > 0	1
$BaSO_4$ (% saturation) > 100	1
CaF_2 (% saturation) > 100	1
SiO_2 (% saturation) > 100	1
Anti-scalants may be required. Consult your anti-scalant manufacturer for dosing and maximum allowable system recovery.	1

RO Chemical Adjustments

	Pass 1 Feed	RO 1st Pass Conc	Pass 2 Feed	RO 2 nd Pass Conc
pH	8.8	8.6	8.6	8.3
Langelier Saturation Index	-0.11	2.14	-3.01	-1.11
Stiff & Davis Stability Index	1.1	2.32	-0.86	0.12
TDS[a] (mg/l)	108.7	2,095	12.80	165.2
Ionic Strength (molal)	0.00	0.03	0.00	0.00
HCO_3^- (mg/L)	48.03	900.3	7.63	97.66
CO_2 (mg/l)	0.11	2.46	0.03	0.79
CO_3^{-2} (mg/L)	1.97	48.12	0.16	1.18
$CaSO_4$ (% saturation)	0.00	1.2	0.00	0.00
$BaSO_4$ (% saturation)	3.3	475.0	0.00	0.04
$SrSO_4$ (% saturation)	0.01	1.1	0.00	0.00
CaF_2 (% saturation)	0.02	205.2	0.00	0.05
SiO_2 (% saturation)	8.9	199.8	0.57	11.3
$Mg(OH)_2$ (% saturation)	0.09	1.2	0.00	0.00

Footnotes:

[a]Total Dissolved Solids includes ions, SiO_2 and B. It does not include NH_3 and CO_2

RO Utility and Chemical Costs

Service Water

	Flow Rate (m^3/h)	Unit Cost ($/m^3$)	Hourly Cost ($/h)	Daily Cost ($/d)
Non-Product Feed Water				
Pass 1	6.3	0.1400	0.89	21.26
Pass 2	0.0	0.1400	0.00	0.00
Total Non-product Feed Water Cost	6.3		0.89	21.26
Waste Water Disposal				
Pass 1	6.3	0.6900	4.37	104.78
Pass 2	0.0	0.6900	0.00	0.00
Total Waste Water Disposal	6.3		4.37	104.78
Total Service Water Cost				126.04

Electricity

Peak Power	(kW)	96.1
Energy	(kWh/d)	2,307
Electricity Unit Cost	($/kWh)	0.0900
Electricity Cost	($/d)	207.6
Specific Energy	(kWh/m^3)	0.79

Pump	Flow Rate (m^3/h)	Power (kW)	Energy (kWh/d)	Cost ($/d)
Pass 1				
Feed	159.58	52.36	1,256.64	113.10

Pass 1 Total		52.36	1,256.64	113.10
Pass 2				
Feed	100.66	43.76	1,050.25	94.52
Pass 2 Total		43.76	1,050.25	94.52
System Total		96.12	2,306.89	207.62

Chemical

Chemical	Unit Cost ($/kg)	Dose 100% (mg/L)	Volume (L/d)	Cost ($/d)
Total Chemical Cost				0.0

Utility and Chemical Cost	($/d)	333.6
Specific Water Cost	($/m³)	0.114